INSTITUTE OF PHYSICS PUBLISHING MEASUREMENT SCIENCE AND TECHNOLOGY

Meas. Sci. Technol. **17** (2006) R175–R195 doi:10.1088/0957-0233/17/12/R01

REVIEW ARTICLE

Energy harvesting vibration sources for microsystems applications

S P Beeby, M J Tudor and N M White

School of Electronics and Computer Science, University of Southampton, Southampton SO17 1BJ, UK

Received 3 March 2005, in final form 19 July 2006
Published 26 October 2006
Online at stacks.iop.org/MST/17/R175

Abstract

This paper reviews the state-of-the art in vibration energy harvesting for wireless, self-powered microsystems. Vibration-powered generators are typically, although not exclusively, inertial spring and mass systems. The characteristic equations for inertial-based generators are presented, along with the specific damping equations that relate to the three main transduction mechanisms employed to extract energy from the system. These transduction mechanisms are: piezoelectric, electromagnetic and electrostatic. Piezoelectric generators employ active materials that generate a charge when mechanically stressed. A comprehensive review of existing piezoelectric generators is presented, including impact coupled, resonant and human-based devices. Electromagnetic generators employ electromagnetic induction arising from the relative motion between a magnetic flux gradient and a conductor. Electromagnetic generators presented in the literature are reviewed including large scale discrete devices and wafer-scale integrated versions. Electrostatic generators utilize the relative movement between electrically isolated charged capacitor plates to generate energy. The work done against the electrostatic force between the plates provides the harvested energy. Electrostatic-based generators are reviewed under the classifications of in-plane overlap varying, in-plane gap closing and out-of-plane gap closing; the Coulomb force parametric generator and electret-based generators are also covered. The coupling factor of each transduction mechanism is discussed and all the devices presented in the literature are summarized in tables classified by transduction type; conclusions are drawn as to the suitability of the various techniques.

Keywords: energy harvesting review, vibration power, self-powered systems, power scavenging

(Some figures in this article are in colour only in the electronic version)

1. Introduction

Wireless systems are becoming ubiquitous; examples include wireless networking based upon the IEEE 802.11 standard and the wireless connectivity of portable devices and computer peripherals using the Bluetooth standard. The use of wireless devices offers several advantages over existing, wired methodologies. Factors include flexibility, ease of implementation and the ability to facilitate the placement of sensors in previously inaccessible locations. The ability to retrofit systems without having to consider issues such as cabling, offers a significant advantage in applications for areas such as condition-based monitoring (CBM) [1], where embedded wireless microsensors can provide continuous monitoring of machine and structural health without the expense and inconvenience of including wiring looms. The

wires (and associated connectors) are often a source of failure in such systems and present a considerable cost issue.

At present, many wireless sensor nodes are battery-powered and operate on an extremely economical energy budget since continuous battery replacement is not an option for networks with thousands of physically embedded nodes [2]. Some specific examples of wireless sensor networks include the WiseNET platform developed by the Swiss Centre for Electronics and Microtechnology (CSEM) [3] and those discussed by Warneke *et al* [4] and Callahan [5]. The low-power characteristics of wireless sensor network components and the design of the system architecture are crucial to the longevity of the sensor nodes. The most power hungry aspect is the wireless communication. Examples of low-power wireless sensor protocols include the IEEE 802.15.4 [6] specification, Zigbee [7] and the ad hoc network architecture demonstrated by the PicoRadio system developed at Berkeley [8]. Intelligence can also be incorporated at the sensor node to perform signal processing on the raw sensor data, execute communications protocols and manage the node's power consumption [9].

These low-power wireless sensor nodes provide a real incentive for investigating alternative types of power source to traditional batteries. Solutions such as micro fuel cells [10] and micro turbine generators [11], both involve the use of chemical energy and require refuelling when their supplies are exhausted. Such systems are capable of high levels of energy and power density and show good potential for the recharging of, or even replacing, mobile phone or laptop batteries [12]. Renewable power can be obtained by generating electrical energy from light, thermal and kinetic energy present within the sensor's environment. These sources can be used as either a direct replacement or to augment the battery, thereby increasing the lifetime and capability of the network [13–16] and mitigate the environmental impact caused by issues surrounding the disposal of batteries. In this context, solar power is probably the most well known. Solar cells offer excellent power density in direct sunlight but are limited in dim ambient light conditions and are clearly unsuitable in embedded applications where no light may be present, or where the cells can be obscured by contamination. Thermal energy can be conveniently transduced into electrical energy by the Seebeck effect. Early thermoelectric microgenerators produced only a few nW [17] but more recently this approach has been combined with micro-combustion chambers to improve output power to $\sim$1 μW/thermocouple [18, 19].

The subject of this review paper is kinetic energy generators, which convert energy in the form of mechanical movement present in the application environment into electrical energy. Kinetic energy is typically present in the form of vibrations, random displacements or forces and is typically converted into electrical energy using electromagnetic, piezoelectric or electrostatic mechanisms. Suitable vibrations can be found in numerous applications including common household goods (fridges, washing machines, microwave ovens etc), industrial plant equipment, moving structures such as automobiles and aeroplanes and structures such as buildings and bridges [20]. Human-based applications are characterized by low frequency high amplitude displacements [21, 22]. The amount of energy generated by this approach depends fundamentally upon the quantity and form of the kinetic energy available in the application environment and the efficiency of the generator and the power conversion electronics. The following sections will discuss the fundamentals of kinetic energy harvesting and the different transduction mechanisms that may be employed. These mechanisms will then be illustrated by a comprehensive review of generators developed to date.

2. General theory of kinetic energy harvesting

2.1. Transduction mechanisms

Kinetic energy harvesting requires a transduction mechanism to generate electrical energy from motion and the generator will require a mechanical system that couples environmental displacements to the transduction mechanism. The design of the mechanical system should maximize the coupling between the kinetic energy source and the transduction mechanism and will depend entirely upon the characteristics of the environmental motion. Vibration energy is best suited to inertial generators with the mechanical component attached to an inertial frame which acts as the fixed reference. The inertial frame transmits the vibrations to a suspended inertial mass producing a relative displacement between them. Such a system will possess a resonant frequency which can be designed to match the characteristic frequency of the application environment. This approach magnifies the environmental vibration amplitude by the quality factor of the resonant system and this is discussed further in the following section.

The transduction mechanism itself can generate electricity by exploiting the mechanical strain or relative displacement occurring within the system. The strain effect utilizes the deformation within the mechanical system and typically employs active materials (e.g., piezoelectric). In the case of relative displacement, either the velocity or position can be coupled to a transduction mechanism. Velocity is typically associated with electromagnetic transduction whist relative position is associated with electrostatic transduction. Each transduction mechanism exhibits different damping characteristics and this should be taken into consideration while modelling the generators. The mechanical system can be increased in complexity, for example, by including a hydraulic system to magnify amplitudes or forces, or couple linear displacements into rotary generators.

2.2. Power output from a resonant generator

The analysis presented in section 2.2.1 presents the maximum power available in a resonant system. This is based upon a conventional second-order spring and mass system with a linear damper and is most closely suited to the electromagnetic case, since the damping mechanism is proportional to velocity. The general analysis, however, still provides a valuable insight into resonant generators and highlights some important aspects that are applicable to all transduction mechanisms. The damping factors of each transduction mechanism are discussed in more detail in section 2.2.2.

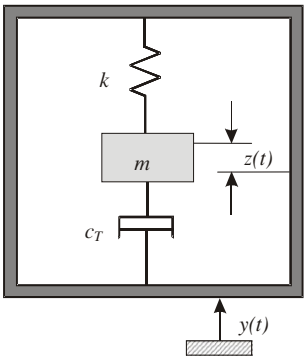

Figure 1. Model of a linear, inertial generator.

2.2.1. General resonant generator theory. Inertial-based generators are essentially second-order, spring-mass systems. Figure 1 shows a general example of such a system based on a seismic mass, m, on a spring of stiffness, k. Energy losses within the system (comprising parasitic losses, c_p, and electrical energy extracted by the transduction mechanism, c_e) are represented by the damping coefficient, c_T. These components are located within the inertial frame which is being excited by an external sinusoidal vibration of the form $y(t) = Y\sin(\omega t)$. This external vibration moves out of phase with the mass when the structure is vibrated at resonance resulting in a net displacement, $z(t)$, between the mass and the frame. Assuming that the mass of the vibration source is significantly greater than that of the seismic mass and therefore not affected by its presence, and also that the external excitation is harmonic, then the differential equation of motion is described as

$$m\ddot{z}(t) + c\dot{z}(t) + kz(t) = -m\ddot{y}(t). \tag{1}$$

Since energy is extracted from relative movement between the mass and the inertial frame, the following equations apply. The standard steady-state solution for the mass displacement is given by

$$z(t) = \frac{\omega^2}{\sqrt{\left(\frac{k}{m} - \omega^2\right)^2 + \left(\frac{c_T\omega}{m}\right)^2}} Y\sin(\omega t - \phi), \tag{2}$$

where ϕ is the phase angle given by

$$\phi = \tan^{-1}\left(\frac{c_T\omega}{(k - \omega^2 m)}\right). \tag{3}$$

Maximum energy can be extracted when the excitation frequency matches the natural frequency of the system, ω_n, given by

$$\omega_n = \sqrt{k/m}. \tag{4}$$

The power dissipated within the damper (i.e. extracted by the transduction mechanism and parasitic damping mechanisms) is given by [23]

$$P_d = \frac{m\zeta_T Y^2\left(\frac{\omega}{\omega_n}\right)^3\omega^3}{\left[1 - \left(\frac{\omega}{\omega_n}\right)^2\right]^2 + \left[2\zeta_T\left(\frac{\omega}{\omega_n}\right)\right]^2}, \tag{5}$$

where ζ_T is the total damping ratio ($\zeta_T = c_T/2m\omega_n$). Maximum power occurs when the device is operated at ω_n and in this case P_d is given by the following equations:

$$P_d = \frac{mY^2\omega_n^3}{4\zeta_T} \tag{6}$$

$$P_d = \frac{mA^2}{4\omega_n\zeta_T}. \tag{7}$$

Equation (7) uses the excitation acceleration levels, A, in the expression for P_d which is simply derived from $A = \omega_n^2 Y$. Since these are steady-state solutions, power does not tend to infinity as the damping ratio tends to zero. The maximum power that can extracted by the transduction mechanism can be calculated by including the parasitic and transducer damping ratios as

$$P_e = \frac{m\zeta_e A^2}{4\omega_n(\zeta_p + \zeta_e)^2}, \tag{8}$$

P_e is maximized when $\zeta_p = \zeta_e$. Some parasitic damping is unavoidable and it may be useful to be able to vary damping levels. For example, it may indeed be useful in maintaining $z(t)$ within permissible limits. However, conclusions should not be drawn without considering the frequency and magnitude of the excitation vibrations and the maximum mass displacement $z(t)$ possible. Provided sufficient acceleration is present, increased damping effects will result in a broader bandwidth response and a generator that is less sensitive to frequency. Excessive device amplitude can also lead to nonlinear behaviour and introduce difficulties in keeping the generator operating at resonance. It is clear that both the frequency of the generator and the level of damping should be designed to match a particular application in order to maximize the power output. Furthermore, the mass of the mechanical structure should be maximized within the given size constraints in order to maximize the electrical power output. It should also be noted that the energy delivered to the electrical domain will not necessarily all be usefully harvested (e.g., coil losses).

Since the power output is inversely proportional to the natural frequency of the generator for a given acceleration, it is generally preferable to operate at the lowest available fundamental frequency. This is compounded by practical observations that acceleration levels associated with environmental vibrations tend to reduce with increasing frequency. Application vibration spectra should be carefully studied before designing the generator in order to correctly identify the frequency of operation given the design constraints on generator size and maximum permissible $z(t)$.

2.2.2. Transduction damping coefficients. The damping coefficient arising from electromagnetic transduction c_e can be estimated from [24]

$$c_e = \frac{(NlB)^2}{R_{load} + R_{coil} + j\omega L_{coil}}, \tag{9}$$

where N is the number of turns in the generator coil, l is the side length of the coil (assumed square), and B is the flux density to which it is subjected and R_{load}, R_{coil} and L_{coil} are the load resistance, coil resistance and coil inductance, respectively. Equation (9) is an approximation and only ideal for the case where the coil moves from a high field region B, to a zero field region. A more precise value for the electromagnetic damping should be determined from finite-element analysis.

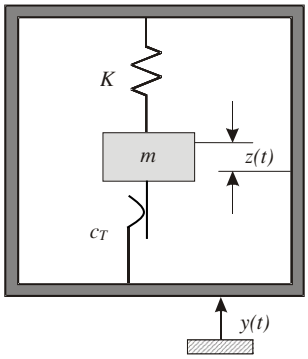

Figure 2. Model of an electrostatic resonant generator.

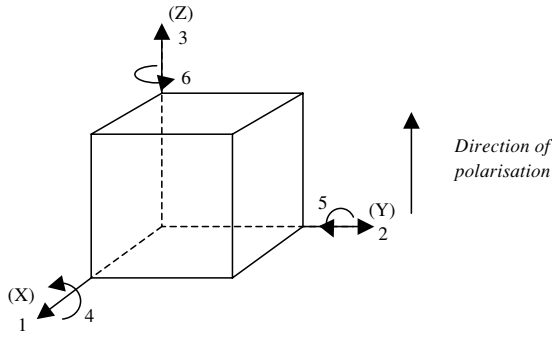

Figure 3. Notation of axes.

Equation (9) shows that R_{load} can be used to adjust c_{e} to match c_{p} and therefore maximize power, although this must be done with the coil parameters in mind. It can be shown that the optimum R_{load} can be found from equation (10) and maximum average power delivered to the load can be found from equation (11) [25]:

$$R_{\text{load}} = R_{\text{coil}} + \frac{(NlB)^2}{c_{\text{p}}}, \tag{10}$$

$$P_{\text{eloadmax}} = \frac{mA^2}{16\zeta_{\text{p}}\omega_{\text{n}}}\left(1 - \frac{R_{\text{coil}}}{R_{\text{load}}}\right). \tag{11}$$

An expression for the piezoelectric damping coefficient is [26]

$$c_{\text{e}} = \frac{2m\omega_{\text{n}}^2 k^2}{2\sqrt{\omega_{\text{n}}^2 + (1/(R_{\text{load}}C_{\text{load}})^2)}}, \tag{12}$$

where k is the piezoelectric material electromechanical coupling factor and C_{load} is the load capacitance. Again R_{load} can be used to optimize ζ_e and the optimum value can be found from equation (13) and as stated previously, maximum power occurs when ζ_{e} equals ζ_{p}.

$$R_{\text{opt}} = \frac{1}{\omega_{\text{n}}C}\frac{2\zeta_{\text{p}}}{\sqrt{4\zeta_{\text{p}}^2 + k^4}}. \tag{13}$$

Electrostatic transduction is characterized by a constant force damping effect, denoted as Coulomb damping and the basic system is shown in figure 2 [27].

The energy dissipated within the damper, and therefore the power, is given by the force–distance product shown in equation (14) where $\omega_{\text{c}} = \omega/\omega_{\text{n}}$ and $U = (\sin(\pi/\omega_{\text{c}})/[1 + \cos(\pi/\omega_{\text{c}})])$:

$$P = \frac{4y_0 F\omega\omega_{\text{c}}^2}{2\pi}\left[\frac{1}{1-\omega_{\text{c}}^2} - \left(\frac{F}{mY_0\omega^2\omega_{\text{c}}}U\right)^2\right]^{1/2}. \tag{14}$$

The optimum damping force is given by

$$F_{\text{opt}} = \frac{y_0\omega^2 m}{\sqrt{2}}\frac{\omega_{\text{c}}}{\left|\left(1-\omega_{\text{c}}^2\right)U\right|}. \tag{15}$$

The application of these equations to practical applications is quite involved and beyond the scope of this review. The paper by Mitcheson *et al* [27] should be studied if further detail is required.

3. Piezoelectric generators

3.1. Introduction

Piezoelectric ceramics have been used for many years to convert mechanical energy into electrical energy. The following sections describe the range of piezoelectric generators described in the literature to date. For the purposes of this review, piezoelectric generators have been classified by methods of operation and applications and include both macro scale (>cm) and micro scale (μm to mm) devices. It begins with a brief description of piezoelectric theory in order to appreciate the different types of generator and the relevant piezoelectric material properties.

3.2. Piezoelectricity

The piezoelectric effect was discovered by J and P Curie in 1880. They found that if certain crystals were subjected to mechanical strain, they became electrically polarized and the degree of polarization was proportional to the applied strain. Conversely, these materials deform when exposed to an electric field. Piezoelectric materials are widely available in many forms including single crystal (e.g. quartz), piezoceramic (e.g. lead zirconate titanate or PZT), thin film (e.g. sputtered zinc oxide), screen printable thick-films based upon piezoceramic powders [28, 29] and polymeric materials such as polyvinylidenefluoride (PVDF) [30].

Piezoelectric materials typically exhibit anisotropic characteristics, thus, the properties of the material differ depending upon the direction of forces and orientation of the polarization and electrodes. The anisotropic piezoelectric properties of the ceramic are defined by a system of symbols and notation [31]. This is related to the orientation of the ceramic and the direction of measurements and applied stresses/forces. The basis for this is shown in figure 3.

The level of piezoelectric activity of a material is defined by a series of constants used in conjunction with the axes notation. The piezoelectric strain constant, d, can be defined as

$$d = \frac{\text{strain developed}}{\text{applied field}}\ \text{m/V}, \tag{16}$$

$$d = \frac{\text{short circuit charge density}}{\text{applied stress}}\ \text{C/N}. \tag{17}$$

Piezoelectric generators that rely on a compressive strain applied perpendicular to the electrodes exploit the d_{33} coefficient of the material whilst those that apply a transverse strain parallel to the electrodes utilize the d_{31} coefficient. The power output achieved in the compressive mode can be improved by increasing the piezoelectric element's thickness or by using multi-layer stacks. Compressive loading, however, is not a practical coupling mechanism for vibration energy harvesting in the majority of applications. Typically, in the case of piezoelectric films or piezoelectric elements bonded onto substrates, the elements are coupled in the transverse direction. Such an arrangement provides mechanical amplification of the applied stresses.

Another important constant affecting the generation of electrical power is the electro-mechanical coupling coefficient, k. This describes the efficiency with which the energy is converted by the material between electrical and mechanical forms in a given direction. This is defined in equation (18) where W_i^{e} is the electrical energy stored in the i axis and W_j^{m} is the mechanical input energy in the j axis.

$$k_{ij}^2 = \frac{W_i^{\mathrm{e}}}{W_j^{\mathrm{m}}}. \tag{18}$$

Furthermore, k_{p} is defined as the planar coupling factor, which is typically used for radial modes of thin discs, and k_{t} is defined as the thickness mode coupling factor for a plate or disk. The efficiency of energy conversion, η, for a piezoelectric element clamped to a substrate and cyclically compressed at its resonant frequency [32] is given in equation (19) where Q is the quality factor of the generator. This relationship suggests that the efficiency is improved by increasing k and Q, which provides a useful guideline when choosing materials and designing generators.

$$\eta = \frac{\frac{k^2}{2(1-k^2)}}{\frac{1}{Q} + \frac{k^2}{2(1-k^2)}}. \tag{19}$$

Goldfarb *et al* [33] have investigated the efficiency of a piezoelectric stack operated in compression. It was found that the efficiency was maximized at frequencies several orders of magnitude below the resonant frequency (e.g. around 5 Hz). This is due to the capacitance of the piezoelectric stack, which is in parallel with the load. Efficiency was also found to increase with increasing force and load resistance but these factors are less significant than frequency.

Other relevant piezoelectric constants include the permittivity of the material, ε, which is defined as the dielectric displacement per unit electric field and compliance, s, which is the strain produced per unit of stress. Lastly, the piezoelectric voltage constant, g, is defined as the electric field generated per unit of mechanical stress, or the strain developed for an applied charge density. These constants are anisotropic and are further defined using the system of subscripts described above. For a more complete description of the constants the reader is referred to the IEEE standards [34].

The piezoelectric properties vary with age, stress and temperature. The change in the properties of the piezoceramic with time is known as the ageing rate and is dependant on the construction methods and the material type. The changes in the material tend to be logarithmic with time, thus the material properties stabilize with age, and manufacturers usually specify the constants of the device after a specified period of time. The ageing process is accelerated by the amount of stress applied to the ceramic and this should be considered in cyclically loaded energy harvesting applications. Soft piezoceramic compositions, such as PZT-5H, are more susceptible to stress induced changes than the harder compositions such as PZT-5A. Temperature is also a limiting factor with piezoceramics due to the Curie point. Above this limit the piezoelectric material will lose its piezoelectric properties effectively becoming de-polarized. The application of stress can also lower this Curie temperature.

Table 1. Coefficients of common piezoelectric materials [35, 36].

Property	PZT-5H	PZT-5A	$BaTiO_3$	PVDF
d_{33} (10^{-12} C N^{-1})	593	374	149	−33
d_{31} (10^{-12} C N^{-1})	−274	−171	78	23
g_{33} (10^{-3} V m N^{-1})	19.7	24.8	14.1	330
g_{31} (10^{-3} V m N^{-1})	−9.1	−11.4	5	216
k_{33}	0.75	0.71	0.48	0.15
k_{31}	0.39	0.31	0.21	0.12
Relative permittivity ($\varepsilon/\varepsilon_{\mathrm{o}}$)	3400	1700	1700	12

The piezoelectric constants for common materials, soft and hard lead zirconate titanate piezoceramics (PZT-5H and PZT-5A), barium titanate ($BaTiO_3$) and polyvinylidene fluoride (PVDF), are given in table 1.

3.3. Impact coupled devices

The earliest example of a piezoelectric kinetic energy harvesting system extracted energy from impacts. Initial work explored the feasibility of this approach by dropping a 5.5 g steel ball bearing from 20 mm onto a piezoelectric transducer [37]. The piezoelectric transducer consisted of a 19 mm diameter, 0.25 mm thick piezoelectric ceramic bonded to a bronze disc 0.25 mm thick with a diameter of 27 mm. This work determined that the optimum efficiency of the impact excitation approach is 9.4% into a resistive load of 10 kΩ with most of the energy being returned to the ball bearing which bounces off the transducer after the initial impact. If an inelastic collision occurred, simulations predicted an efficiency of 50% assuming a 'moderate' system Q-factor and typical electromechanical coupling and dielectric loss factors based upon PZT. Later research further explored the feasibility of storing the charge on a capacitor or battery [38]. The output of the generator was connected in turn to 0.1, 1 and 10 μF capacitors via a bridge rectifier. The ability of the generator to charge the capacitors depended upon the value of the capacitor and its initial voltage. Optimum efficiency was found to occur with a capacitor value of 1 μF for multiple impacts, but larger capacitors can obviously store more energy. The generator was also attached to nickel cadmium, nickel metal hydride and lithium ion batteries with a range of capacities. The charging characteristics were found to be unaffected by the battery type or capacity and were very similar to that of a 10 μF capacitor. The time taken for this approach to recharge the batteries was not determined.

Recent work by Cavalier *et al* has explored the coupling of mechanical impact to a piezoelectric (PZT) plate via a nickel package [39]. The impact occurs on the outside of the nickel

case (an HC45 package, typically used for vacuum packaging quartz resonators) and the vibrations are transmitted to the piezoelectric element. This work investigated the optimum mounting arrangements for the piezoelectric plate and the inclusion of a silicon beam sandwiched between two PZT plates forming a resonant structure. The device was tested by dropping a 40 g tin ball from the heights of 1 cm and 3 cm (3.92 and 11.7 μJ impact energy respectively). The electrical energy generated was found to vary linearly with incident energy. The inclusion of the silicon beam within the package was found to improve the magnitude and duration of the electrical output compared to the basic PZT plate arrangement. Over 2 V was generated for each 11.7 μJ impact with a total package size of 120 mm^3.

Xu *et al* [40] have compared the efficiency of impact stressing a piezoelectric ceramic versus slow compressive loading. The impacts were generated by dropping a steel ball onto a clamped piezoceramic whilst the compressive loading involved cyclical application of a compressive stress of up to 28 MPa over a 2 s period. The stresses within the piezoceramic were maintained within the linear region and the properties of the piezoelectric were unaffected by the experiment. The slowly applied stress was found to produce more energy than the impact stress although voltage levels were comparable. Impact stressing of piezoceramics was found to be problematic due to their brittle nature and the poor efficiency of the mechanical energy transfer between the impact and the sample.

The efficiency of lithium niobate ($LiNbO_3$) plates under impact excitation has also been evaluated by Funasaka *et al* [41]. $LiNbO_3$ was chosen because it has a higher coupling factor k and intrinsic quality factor Q. The efficiencies of PZT and $LiNbO_3$ plates were compared under impact conditions and were calculated to be 65% and 78% respectively. This work claimed an impact excitation efficiency of 70%, which is higher than other reported values. Since the dielectric constant of $LiNbO_3$ is less than PZT the amount of electrical energy generated is actually less than the PZT case. Energy generation can be improved by using a multilayered $LiNbO_3$ but this does reduce efficiency due to the influence of the bonding layers used in the fabrication of the stack.

3.4. Human powered piezoelectric generation

The use of piezoelectric generators to power human-wearable systems has been extensively studied. Human motion is characterized by large amplitude movements at low frequencies and it is therefore difficult to design a miniature resonant generator to work on humans. Coupling by direct straining of, or impacting on, a piezoelectric element has been applied to human applications and these are detailed below.

Studies have shown that an average gait walking human of weight 68 kg, produces 67 W of energy at the heel of the shoe [42]. Whilst harvesting this amount of energy would interfere with the gait, it is clear that extracting energy from a walking person presents a potential energy harvesting opportunity. The theoretical limits of piezoelectric energy harvesting on human applications based upon assumptions about conversion efficiencies have suggested that 1.27 W could be obtained from walking [36]. One of the earliest examples of a shoe-mounted generator incorporated a hydraulic system mounted in the heel and sole of a shoe coupled to cylindrical PZT stacks [43]. The hydraulic system amplifies the force on the piezoelectric stack whilst reducing the stroke. Initial calculations were performed in order to design a generator capable of developing 10 W. A 1/17th scale model was built and tested and was found to generate 5.7 ± 2.2 mW kg^{-1} whilst walking, which suggested that 6.2 W could be generated with the full size generator on a 75 kg subject. The generator design was relatively large in size and the intended power levels are likely to interfere with the gait of the user.

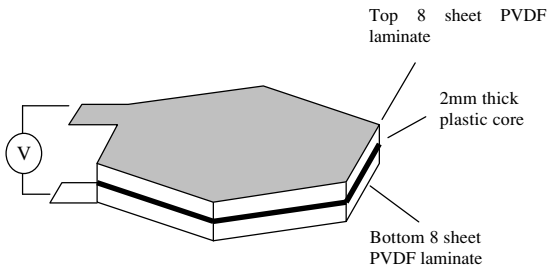

Figure 4. PVDF shoe insole (after Kymiss *et al* [44]).

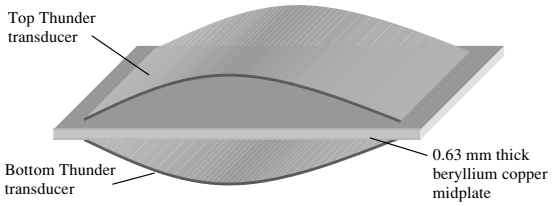

Figure 5. Schematic of the piezoelectric dimorph (after Shenck *et al* [45]).

A subsequent device has been developed at the Massachusetts Institution of Technology (MIT) in the 1990s [44]. Researchers first mounted an 8 layer stack of PVDF laminated with electrodes either side of a 2 mm thick plastic sheet (see figure 4). This stave was used as an insole in a sports training shoe where the bending movement of the sole strains both PVDF stacks producing a charge from the d_{31} mode. At a frequency of a footfall of 0.9 Hz, this arrangement produced an average power of 1.3 mW into a 250 kΩ load. A second approach involved the use of a compressible dimorph (see figure 5) located in the heel of a Navy work boot that generated energy from the heel strike [45]. The dimorph incorporated two Thunder TH-6R piezoelectric transducers manufactured by Face International Corporation [46]. The Thunder transducers are pre-stressed assemblies of stainless steel, PZT and aluminium which are bonded together at elevated temperature using a NASA patented polyimide adhesive LaRC^{TM}-SI. The differential thermal expansion coefficients of the materials result in a characteristic curved structure with the PZT layer being compressively stressed enabling it to deform to a far greater extent than standard PZT structures. As the heel of the shoe hits, the transducers are forced to deform and, as the heel is lifted, the transducers spring back into their original shape. Each event results in a voltage being generated and with an excitation of 0.9 Hz the dimorph produces an average of 8.4 mW power into a 500 kΩ load.

Simply supported curved piezoelectric unimorphs similar to that shown in figure 5 have been modelled in more detail by Yoon *et al* [47]. The basic rules of thumb identified by the modelling suggested that it is more effective to increase the width of the unimorph rather than the length and that the height at the centre and the thickness of the substrate material should be maximized within the capability of the manufacturing process and the available compressing force. These rules were validated by a simple test comprising the placement of Thunder transducers under the heel of a 100 lb (45 kg) subject.

PVDF inserts have more recently been studied analytically by Mateu [48] who compared homogeneous (two layers of PVDF bonded together) with heterogeneous beams (PVDF bimorph) with different boundary conditions (cantilever and simply supported) and both rectangular and triangular shapes. These cantilevers were considered to be located within a cavity in the sole of a shoe, with the ultimate deflection limited by the cavity dimensions. The overall conclusion was that the best PVDF structure was a simply supported asymmetric bimorph beam with a distributed load with a large ratio of substrate to PVDF thickness being preferable.

Piezoelectric crystals embedded in the heel of a shoe have also been demonstrated in the UK by the Electric Shoe Company. This approach was evaluated by recharging a mobile phone after 5 days walking [49].

Piezoelectric energy harvesting for *in vivo* applications has been explored by Ramsay and Clark [50]. The motivation of this work was the potential for *in vivo* 'lab on a chip' or other systems powered from kinetic energy sources present within the subject. The design used a square plate geometry to extract energy from the change of blood pressure with each pulse. A typical blood pressure change of 40 mmHg at a frequency of 1 Hz was used to calculate the power of a range of square plates from 9 μm to 1100 μm thick and with 1 mm to 1 cm side lengths. Maximizing the area and minimizing the plate thickness maximized the calculated power providing a theoretical value of 2.3 μW. Circular and square PVDF plates for use in harvesting energy from changes in blood pressure have also been investigated by Sohn *et al* [51]. The finite-element analysis of the PVDF membranes determined that for a circular diaphragm of 5.56 mm radius the optimum thickness of 9 μm produces 0.61 μW whilst a 10 $\times$ 10 mm square membrane of thickness 110 μm produces 0.03 μW. Experimental tests using 28 μm thick membranes pulsed at 60 Hz by 5333 N m^{-2} uniform pressure yielded 0.34 μW and 0.25 μW for the circular and square plates, respectively. These values could clearly have been increased by employing patterned electrodes and differential poling as shown in figure 13 and discussed in section 3.6.

The generation of power by positioning piezoelectric inserts within orthopaedic implants has been studied by Platt *et al* [52]. These inserts are intended to power sensors that provide *in vivo* monitoring of the implant in order to reduce future complications. The axial force across a knee joint can reach three times body weight several times per step and this load was applied across a prototype generator containing three 1 $\times$ 1 $\times$ 2 cm piezoelectric stacks each containing $\sim$145 PZT layers. The implant was demonstrated with a 10 μF storage capacitor and a microprocessor periodically switching an LED on during each step. The system was found to deliver 850 μW of continuous regulated power with an electrical efficiency of 19% with the maximum mechanical efficiency being $\sim$20% into impedance matched load. Longevity tests suggest the generator should be capable of producing useful power for tens of millions of cycles.

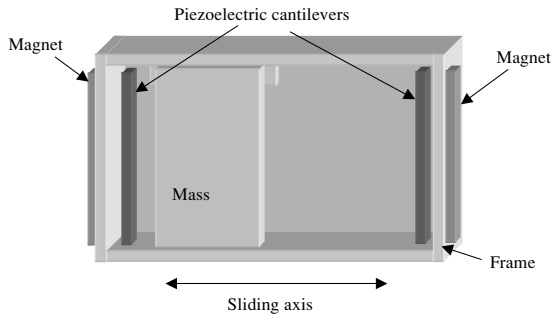

Figure 6. Bi-stable piezoelectric generator designed for human applications.

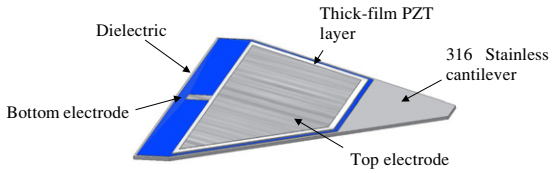

Figure 7. Tapered thick-film PZT generator (not to scale) after Glynne-Jones *et al* [55].

Impact coupling of a piezoelectric transducer designed for use in human applications has been described by Renaud *et al* [53]. The device comprised an inertial mass confined within a frame but free to slide along one axis. The steel inertial mass was 2 mm long in the sliding axis, 10 mm wide and 5 mm thick and had a mass of 750 mg. The frame was 12 mm long in the sliding axis and 10 mm wide. Energy is generated when the sliding mass strikes steel/PZT cantilevers located at each end of the frame. In order to increase the power output and achieve bi-stable operation, holding magnets were positioned at each end of the frame as shown in figure 6. Modelling results predict that the device will generate up to 40 μW of useful electrical power from a volume of 1 cm^3 given excitation amplitudes of 10 cm at 1 Hz (0.1 m s^{-2}).

3.5. *Cantilever-based piezoelectric generators*

A cantilever structure with piezoelectric material attached to the top and bottom surfaces is an attractive geometry for harvesting energy from vibrations. The structure is designed to operate in a bending mode thereby straining the piezoelectric films and generating a charge from the d_{31} effect. A cantilever provides low resonant frequencies, reduced further by the addition of a mass on the end of the beam, in a low volume structure and high levels of strain in the piezoelectric layers.

A tapered cantilever beam was developed by Glynne-Jones *et al* and is shown in figure 7 [54–56]. The tapered profile ensures a constant strain in the piezoelectric film along its length for a given displacement. The generator was fabricated by screen printing a piezoelectric material onto a 0.1 mm thick hardened AISI 316 stainless steel. The piezoelectric

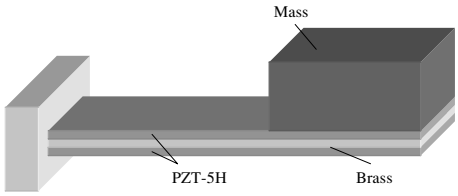

Figure 8. Schematic of cantilever piezoelectric generator developed by Roundy *et al* [59].

material is based upon PZT-5H powder blended with Corning 7575 glass and a suitable thick-film vehicle to form a screen printable thixotropic paste [57]. This was printed on both sides of the steel cantilever to cancel the uneven thermal expansion coefficients and maximize the power generated. The structure operated in its fundamental bending mode at a frequency of 80.1 Hz and produced up to 3 μW of power into an optimum resistive load of 333 kΩ. The thick-film printing of piezoelectric material is a low cost batch process but the power generated is limited by the reduced piezoelectric properties of the material compared to that of bulk piezoceramics. Recent advances in the film properties will improve power output [58].

Another composite piezoelectric cantilever beam generator has been developed by Roundy and Wright [20, 59]. The cantilever used was of constant width which simplifies the analytical model and beam fabrication but results in an unequal distribution of strain along its length. For a detailed analysis of the mathematical models presented the reader is referred to [59]. A prototype generator was fabricated by attaching a PZT-5A shim to each side of a steel centre beam. A cubic mass made from an alloy of tin and bismuth was attached to the end and the generator tuned to resonate at 120 Hz. The prototype produced a maximum power output of nearly 80 μW into a 250 kΩ load resistance with 2.5 m s^{-2} input acceleration and the results showed a reasonable level of agreement with the analytical models. These models were then used to optimize the generator design within an overall size constraint of 1 cm^3. Two designs were adopted, each using PZT-5H attached to a 0.1 mm thick central brass shim (see figure 8). Design 2 using a PZT thickness of 0.28 mm, possessing a beam length of 11 mm and a tungsten proof mass of 17 $\times$ 7.7 $\times$ 3.6 mm, produced 375 μW with an input acceleration of 2.5 m s^{-2} at 120 Hz. This generator was demonstrated powering a radio transceiver with a capacitor used for energy storage and achieved a duty cycle of 1.6%. This work concluded that the generator output at resonance is proportional to the mass attached to the cantilever and this should be maximized provided size and strain constraints are not exceeded.

Piezoelectric cantilever generators have also been investigated by Sodano *et al* [60]. An alternative mathematical analysis uses energy methods to arrive at the constitutive equations of a cantilever PZT bimorph similar to that shown in figure 8 but with no mass and the PZT not extending to the end of the beam. Models were validated by evaluating a Quick Pack QP40 N (Mide Technology Corporation) piezoelectric actuator clamped at one end and placed on a shaker. The transducer is a composite formed from four piezoceramic elements embedded in a Kapton and epoxy matrix. The model is able to predict the current output for a given excitation frequency and amplitude and the results were within 4.61% of the experimental values. The efficiency of the conversion and the degree of damping is not only dependant upon the transducer but also the associated circuitry. The influence of the input impedance on system damping was evaluated and optimum efficiency and therefore maximum damping was found to occur at 15 kΩ. This value will be particular to the transducer and is matched to the impedance of the device. The Mide Technology Corporation has since marketed a vibration energy harvesting device based upon a cantilevered Quick Pack transducer with an inertial mass clamped to the free end [61]. The device is 3.6 $\times$ 1.7 $\times$ 0.39 inches in size and generates 500 μW at 113 Hz and 1g acceleration.

Sodano *et al* have also investigated the amount of power generated through the vibration of a composite piezoelectric aluminium plate and have compared two methods of power storage [62]. A Piezo Systems PSI-5H4E plate (62 $\times$ 40 $\times$ 0.27 mm) was bonded to an aluminium plate (80 $\times$ 40 $\times$ 1 mm) and excited using an electromagnetic shaker with both resonant and random excitation signals. It was found that the plate could generate a maximum power of 2 mW when excited at its resonant frequency. This paper demonstrated that the power output of a piezoelectric material was able to recharge a fully discharged battery and suggests that batteries are the superior option for storing electrical energy for continuous power supply applications [63]. Capacitors, it is suggested, are better suited to duty cycled applications that only require a periodic power supply

Further modelling and analysis of the influence of load resistance on the output power of cantilevered piezoelectric bimorph generators has been presented by Lu *et al* [64]. The optimum load was found to vary for different piezoelectric generators as shown in equation (20) where t is the thickness of piezoelectric layer, b beam width, L is the length of the piezoelectric film on the beam, ε_{33} the dielectric constant, ω the frequency and C_p is the capacitance of piezoelectric element:

$$R_{opt} = \frac{t}{bL\varepsilon_{33}\omega} = \frac{1}{\omega C_P}. \tag{20}$$

The merits of unimorph versus bimorph cantilevers have been studied by Ng *et al* [65]. Their model assumed an ideal piezoelectric material with properties similar to PZT 5H in table 1 attached to a brass shim in a unimorph and bimorph configuration. The relative merits of the configurations depend upon frequency and load resistance with, generally, the unimorph being most suitable for lower frequencies and load resistances. The bimorph arrangement with the piezo layers in parallel is better suited at mid-range frequencies and load resistances, but the most power is generated with the bimorph connected in series and operated at even higher frequencies and load resistances. Exact values depend upon the design of the generator, but the bimorph in series was best for the largest range of frequencies and resistances.

Cantilevered piezoelectric unimorphs have also been coupled to radioactive sources in order to achieve a method of excitation that does not rely on environmental vibrations [66, 67]. The principle uses the radiated β particles to electrostatically charge a conductive plate on the underside of a piezoelectric unimorph. As the electrostatic field builds, the

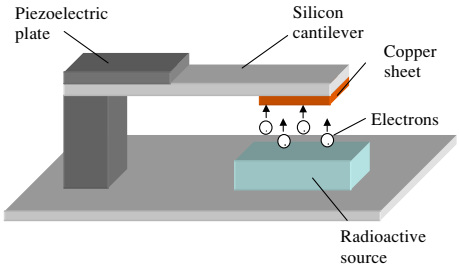

Figure 9. Radiation-driven piezoelectric generator.

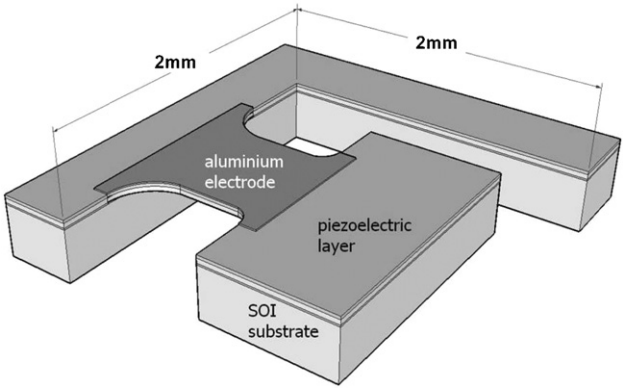

Figure 10. Micromachined silicon cantilever mass piezoelectric generator.

beam is attracted to the source until the contact is made and the field dissipated. At this point, the beam is released to vibrate at its natural frequency and the kinetic energy harvested from the piezoelectric film. A schematic of the device is shown in figure 9. Different material combinations, device geometries and radioisotopes can alter the output and characteristics of the generator. For example, a 1 cm^2 0.5 millicurie thin film ^{63}Ni source with a half life of 100.2 years coupled to a 15 mm long, 2 mm wide silicon cantilever produced a peak power of 16 μW with a reciprocation period of 115 min [68]. Whilst this presents a novel and repeatable method for exciting the cantilevers vibrations, the power output is very periodic and, when averaged out over a given time period, very low (<1 nW).

A micromachined silicon MEMS version of the cantilever mass geometry has been developed under a project funded by the European Union framework 6 programme entitled vibration energy scavenging (VIBES). The device, shown in figure 10, consists of a 1.5 mm × 0.75 mm area inertial mass deep reactive ion etched (DRIE) from an SOI wafer with a 400 μm thick handle wafer, 2 μm thick buried oxide and a 5 μm thick top silicon layer. The supporting cantilever is fabricated from the top silicon layer only and is 750 μm long. The structure has been simulated with 1 μm thick layers of aluminium nitride (AlN) and PZT piezoelectric materials. Modelling results predicted 100 nW for the AlN device and 600 nW for the PZT device at resonant frequencies of approximately 900 Hz [69].

Another MEMS cantilever device has been demonstrated by Jeon *et al* [70]. The cantilever was formed from a membrane made from layers of thermally grown silicon oxide,

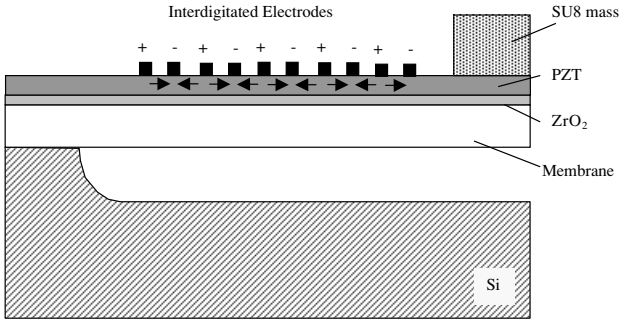

Figure 11. MEMS PZT generator with interdigitated electrodes (after [70]).

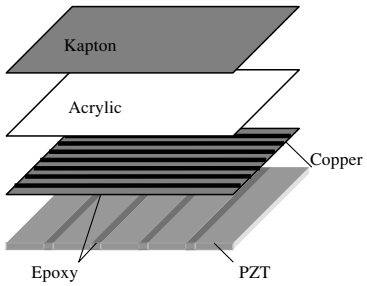

Figure 12. MFC Actuator (after Sodano *et al* [71]).

deposited silicon nitride and sol–gel deposited zirconium dioxide which acts as a buffer layer. The top PZT layer, 0.58 mm thick, was finally deposited again using a sol–gel process. The novelty of this work mainly arises from the use on an interdigitated Ti/Pt electrode pattern e-beam evaporated and patterned on top of the PZT later. This electrode configuration enables the d_{33} and g_{33} coefficient of the PZT, typically 2–2.5 times larger than d_{31} and g_{31}, to be exploited as the beam bends. The beam is released by undercutting the deposited films using a silicon vapour etch to avoid the effects of stiction. A proof mass can be added at the beam tip by defining a feature formed from a thick layer of SU8 photoresist (see figure 11). The generator was found to have a fundamental resonant frequency of 13.9 kHz at which it delivered 1.01 μW at a reported 14 nm base displacement (∼10 m s^{-2} acceleration).

3.6. Other piezoelectric generators

Sodano *et al* also compared macro-fibre composite (MFC) actuators with standard piezoceramics [71, 72]. The MFC structure was developed by NASA [73] and consists of thin PZT fibres embedded in a Kapton film and connected with an interdigitated electrode (IDE) pattern shown in figure 12. When the actuator is bonded to a structure, stresses are coupled along the length of the fibres thereby exploiting the d_{33} properties of the material rather than the lower d_{31}. Despite this, the MFC was found to supply too little current to charge batteries whilst the standard PZT piezoceramic was able to charge various capacity nickel metal hydride batteries. For example, a 200 mA h battery was charged in 4 h. The IDE geometry results in a relatively low-capacitance device compared with a parallel plate with the same piezoelectric

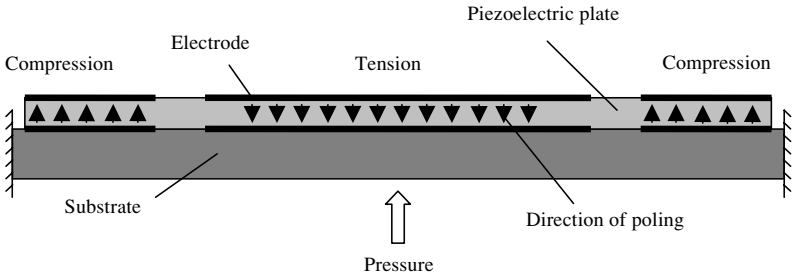

Figure 13. Differential poling of piezoelectric layer bonded to a clamped circular plate.

area. This results in a high impedance at typical excitation frequencies and therefore reduces the useful power output of the generator [74, 75].

Elvin *et al* [76] have explored the possibility of using the energy generated from a piezoelectric sensor to power a wireless link thereby realizing a self-powered wireless strain sensor. A 28 μm thick, 23 mm wide and 40 mm long piece of PVDF was attached to a four-point bending beam subject to cyclical loading. The PVDF element was used not only to measure the resulting strain, but its output was stored in a capacitor. This was used to power a simple air core copper coil in series with a capacitor tuned to 1 MHz which achieved up to 2 m transmission range.

A piezoelectric micromachined ultrasonic transducer (pMUT) has also been demonstrated in an energy scavenging application [77]. The transducer consists of a 1 μm thick circular silicon membrane of 600 μm diameter with a 2 μm thick PZT layer deposited on the top surface. The thermal expansion coefficient mismatches between the materials results in a built in stress within the structure that causes a static deflection of 5.5 μm at the centre of the membrane. This deflection could be above or below the surface of the membrane and the device was therefore found to be bi-stable. The membrane was found to snap from one position to the other by simply rotating the device in Earth's gravitational field with each change in position producing a sharp signal of over 1 V over a 100 μs period. The electrical output is enhanced by the stress stored within the bi-stable structure. This device introduces the very attractive possibility of a non-resonant structure that will respond to any frequency movement of sufficient acceleration. Energy harvesting using circular piezoelectric plates bonded to a clamped circular substrate has also been studied by Kim *et al* [78, 79]. This study has used patterned electrodes and differentially poled regions of the piezoelectric plate to ensure the voltage from the each region are the same polarity despite the opposite stresses induced by an applied pressure (as shown in figure 13). This arrangement would also apply to other clamped–clamped structures such as beams.

Piezoelectric materials have been used to harvest kinetic energy from a range of sources, typically vibration but also fluid flows. The energy harvesting eel uses a PVDF membrane located in the vortex wake of a body located in a fluid stream to generate electricity. The vortices in the wake deform the PVDF membrane which is up to 0.7 mm thick and 0.457 m long [80]. This application is obviously limited to large scale fluidic applications and may find uses in powering ocean sensor buoys.

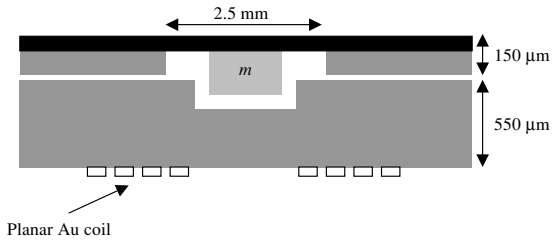

Figure 14. Cross-section of the electromagnetic generator proposed by Williams *et al* [23, 82].

4. Electromagnetic generators

4.1. Introduction

Electromagnetic induction, first discovered by Faraday in 1831, is the generation of electric current in a conductor located within a magnetic field. The conductor typically takes the form of a coil and the electricity is generated by either the relative movement of the magnet and coil, or because of changes in the magnetic field. In the former case, the amount of electricity generated depends upon the strength of the magnetic field, the velocity of the relative motion and the number of turns of the coil.

One of the most effective methods for energy harvesting is to produce electromagnetic induction by means of permanent magnets, a coil and a resonating cantilever beam. In principle, either the magnets or the coil can be chosen to be mounted on the beam while the other remains fixed. It is generally preferable, however, to have the magnets attached to the beam as these can act as the inertial mass. The generalized schematic diagram depicted in figure 1 is applicable to describe the operation of electromagnetic generators. The damper, c, effectively represents the electromagnetic transduction mechanism, i.e. the magnet and coil arrangement.

4.2. Wafer-scale implementations

Figure 14 is a schematic of an electromagnetic approach, which is described by Williams *et al* [81] from the University of Sheffield, UK.

The generator consists of a seismic mass, m, on a spring, k. When the generator is vibrated, the mass moves out of phase with the generator housing, so that there is a net movement between the mass and the housing. This relative displacement is assumed to be sinusoidal in nature and can drive a suitable electromagnetic transducer to generate

electrical energy. The transducer is depicted as a dashpot, d, because the conversion of mechanical energy into electrical energy damps the vibrations. The size of the electromagnetic transducer described by Williams *et al* is around 5 mm × 5 mm × 1 mm. The harmonic analysis was undertaken in order to assess the viability of the device. For a typical device, the predicted power generation was 1 μW for an excitation frequency of 70 Hz, and 100 μW at 330 Hz [83]. Shearwood and Yates from the University of Sheffield, UK [84] have fabricated a generator based on the design. It comprises a flexible circular membrane, which was bulk micromachined on a GaAs substrate coated with a 7 μm layer of polyimide. A SmCo magnet, having a mass of 2.4×10^{-3} kg, was attached to the underside of the membrane. The planar Au coil had 13 turns and was patterned on a separate wafer. The device was tested and generated 0.3 μW at excitation frequency of 4.4 kHz. The measured electrical power output was lower than the predicted value and this was thought to be due to the nonlinear effects of spring stiffening, which occurred as the excitation amplitude was increased.

Another type of resonant microgenerator is described by Mizuno and Chetwynd [85]. Their proposed device comprises a beam with an integrated coil and a fixed external magnet. The dimensions of the cantilever beam were 500 μm × 100 μm × 20 μm and the size of the NdFeB magnet was 30 mm × 10 mm × 6 mm. The resonant frequency of the structure was 58 kHz. A power output of only 6 nW was predicted for a typical single-element electromagnetic microgenerator. The magnitude of the output voltage was estimated as being only 1.4 mV. The authors fabricated a larger version of their proposed device for evaluation purposes. The actual size of the beam was increased to 25 mm × 10 mm × 1 mm and the resulting resonant frequency was 700 Hz. For an input vibration of 0.64 μm, the output power was found to be 0.4 nW. As a result of the low output power, the authors suggest that electromagnetic generators do not offer practical solutions for energy harvesting problems. They may have reached a different conclusion if they had chosen to evaluate a moving-magnet approach as the additional seismic mass would have increased the electrical power available.

Kulah and Najafi describe a silicon-based generator, which comprises two separate chips combined together [86]. Their device utilizes two resonant structures that are designed to achieve mechanical up-frequency conversion. The authors argue that because most silicon structures have relatively high resonant frequencies (several kHz) and a majority of ambient vibration frequencies are less 100 Hz, then a device that can perform mechanical up-frequency conversion will provide an efficient solution to energy harvesting problems. To demonstrate this, they have fabricated a silicon generator that has an upper diaphragm with a resonant frequency of 25 Hz. A NdFeB magnet on the upper diaphragm is used to excite a lower structure into resonance through magnetic attraction. The lower diaphragm has a resonant frequency of around 11 kHz. Integrated coils are fabricated on the lower structure. The authors quote the theoretical maximum power generated as being 2.5 μW, but they only measured 4 nW from a millimetre-scale mock-up. The level of input mechanical excitation is not quoted in the paper.

Huang *et al* have addressed the issue of human-powered electrical generation [87] and discuss a method of using an

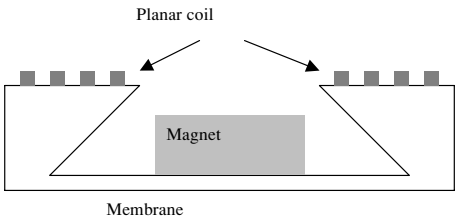

Figure 15. Inertial generator described by Pérez-Rodríguez *et al* [88].

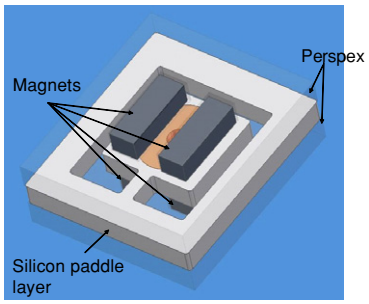

Figure 16. A silicon electromagnetic generator (after Beeby *et al* [90]).

electromagnetic harvester comprising a planar copper coil, a nickel–iron spring element and a magnet. The device has a resonant frequency of 100 Hz and is reported to be capable of generating 0.16 μW for an excitation level provided by a 'finger tap'. A similar structure has been investigated by Pérez-Rodríguez *et al* [88], who have used a polyimide film as the spring, a NdFeB magnet and a planar coil made from a 1.5 μm thick aluminium layer. A cross-section of the device is depicted in figure 15. The quoted power output is 1.44 μW for a displacement of 10 μm and a resonant frequency of 400 Hz. Scherrer *et al* [89] discuss the possibility of using low temperature co-fired ceramics (LTCC) to fabricate a multi-layer screen printed coil. The coil comprises 96 tape layers and has a total of 576 turns. It is held in position between two copper/beryllium springs and is designed to move vertically in response to an input excitation thereby cutting the flux lines of four externally mounted magnets. The theoretical maximum output power is predicted to be 7 mW when operated at the resonant frequency of 35 Hz.

Beeby *et al* have developed a silicon-based generator that comprises micromachined paddle, four NeFeB magnets and a wire-wound coil [90]. The device is shown in figure 16. Two of the magnets are located within etched recesses in the two Pyrex wafers, which are anodically bonded to each face of the silicon wafer. The coil is located on a silicon cantilevered paddle, which is designed to vibrate laterally in the plane of the wafer. The device has a resonant frequency of 9.5 kHz and has been shown to generate 21 nW of electrical power from 1.92 m s^{-2} rms.

4.3. Macro-scale implementations

El-Hami *et al* at the University of Southampton, UK [24] describe the simulation, modelling, fabrication and characterization of a vibration-based electromechanical power

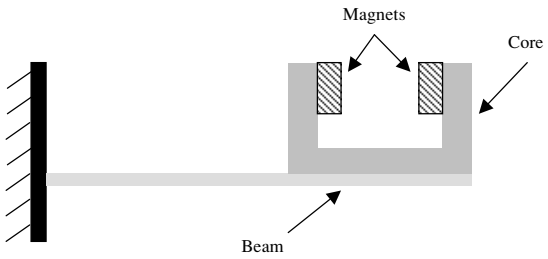

Figure 17. The electromagnetic generator proposed by El-Hami *et al* [24].

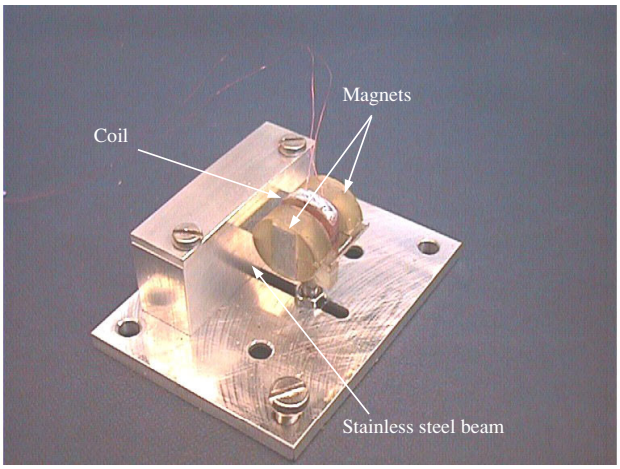

Figure 18. An electromagnetic generator based on four moving magnets and a fixed coil (after Glynne-Jones *et al* [91]).

generator. The device comprises a cantilever beam (spring), fixed at one end and supporting a pair of NdFeB magnets (mass) on a c-shaped core at the free end. The coil is made up of many turns of enamelled copper wire and is fixed in position between the poles of the magnets. The device is depicted in figure 17. It was found that power generation in excess of 1 mW for a volume of 240 mm^3 at a vibration frequency of 320 Hz was obtained.

Glynne-Jones *et al* [91] presented experimental results obtained from prototypes fabricated using batch machining and hand assembly with different magnet configurations. Following the work of El-Hami *et al* [24], the Southampton team have assessed two prototypes, based on a cantilever structure, but having different combinations of magnets and coils. The initial prototype was based on a moving coil between two fixed magnets and had an overall volume of 0.84 cm^3. The second device was a moving four-magnet generator (with a fixed coil), having an overall volume of 3.15 cm^3; this is shown in figure 18. The first prototype generated power levels up to 180 μW, for a free-end beam displacement of 0.85 mm. The second prototype was aimed at improving the magnitude of the output voltage (and hence power) by improving the magnetic coupling between the magnets and coil. In broad terms, for the same input vibration, the second generator produced more than twice the output voltage (1 V compared with a few hundred millivolts) and hence more than four times the instantaneous power. The authors present results showing the response from a generator mounted on the engine block of a car. An instantaneous power of 4 mW was measured during a journey of 1.24 km and the average power was found to be 157 μW.

Amirtharajah and Chandrakasan from the Massachusetts Institute of Technology describe an integrated circuit for low-power DSP applications, which contains a moving coil electromagnetic generator [92]. The resonant frequency of the generator was 94 Hz and the peak output voltage was measured at 180 mV. The authors modelled the generator performance for a human-powered application and predicted that an average of 400 μW could be generated from a 2 cm movement at a frequency of 2 Hz.

Li *et al* from the Chinese University of Hong Kong developed a magnet and coil arrangement, which comprises a laser-micromachined spiral copper spring and NdFeB magnet and a coil, which is fixed in position on the housing of the structure [93]. The device occupies an overall volume of around 1 cm^3 and is capable of producing 2 V at its resonant frequency of 64 Hz. This results in a power output of 10 μW for an excitation amplitude of 100 μm. Ching *et al*, from the same group, discuss a similar generator fabricated on a printed circuit board [94]. An improved spiral spring resulted in a peak-to-peak output voltage of up to 4.4 V and a maximum power of 830 μW when driven by a 200 μm displacement at its resonant frequency of 110 Hz.

4.4. Commercial devices

Several companies specializing in the field of energy harvesting have emerged over recent years. Kinetron [95] is a Dutch manufacturer of precision electromechanical products, who has patented a microgenerator that is capable of harnessing the kinetic energy produced by the movement of the human wrist. They have also developed an electromagnetic rotational generator which can be used in applications such as self-powered pedal lights for bicycles. Despite the absence of specific devices for use as vibration energy scavengers, the company manufactures a variety of different size rotary devices capable of producing output powers in the range of 10–140 mW depending on the rotational speed available. Perpetuum Ltd [96] is a UK-based company that has developed a series of vibration-powered electromagnetic generators which cover a broad range of vibration frequencies. Power outputs of up to 5 mW at an acceleration of 0.1 m s^{-2} have been demonstrated and their devices have been used to power various types of sensor and commercial wireless modules, resulting in battery-less, wireless sensor networks.

5. Electrostatic generators

5.1. Introduction

This section covers electrostatic generators. Initially the basic concepts and operating principles are outlined. There follows a review of the electrostatic-based generators published to date giving their structure and an outline of their performance. Finally a summary table is provided.

5.2. Operating principle

A capacitor consists of two plates which are electrically isolated from each other typically by air, vacuum or an

insulator. The charging of the plates by a battery of voltage V creates equal but opposite charges on the plates, Q, leading to a storage of the charge when the voltage source is disconnected. In MEMS the separation between the two plates is typically very small (nm to μm).

The fundamental definition of the capacitance of such a capacitor is given by

$$C = Q/V, \tag{21}$$

where C is the capacitance in farads, Q is the charge on the plate in coulombs and V is the voltage on the plates in volts. For a parallel plate capacitor, C is given by

$$C = \varepsilon \frac{A}{d}, \tag{22}$$

where ε is the permittivity of the material between the plates in F m^{-1}, A is the area of the plates in m^2 and d is the separation between the plates in m.

If ε_0 is the permittivity of free space, equation (22) can be expressed in terms of the dielectric constant, $\kappa = \varepsilon/\varepsilon_0$, of the insulator material:

$$C = \kappa \varepsilon_0 \frac{A}{d}. \tag{23}$$

The voltage across a parallel plate capacitor is given by

$$V = \frac{Qd}{\varepsilon_0 A}. \tag{24}$$

The energy stored in a capacitor, with plate charge Q and potential difference V, is given by

$$E = 0.5QV = 0.5CV^2 = 0.5Q^2/C. \tag{25}$$

If the charge on the plates is held constant the perpendicular force between the plates is given by

$$F = 0.5Q2d/\varepsilon A. \tag{26}$$

If the voltage between the plates is held constant the perpendicular force between the plates is given by

$$F = 0.5\varepsilon A V^2/d^2. \tag{27}$$

The work done against the electrostatic force between the plates provides the harvested energy.

Electrostatic generators can be classified into three types [97].

1. In-plane overlap varying.
2. In-plane gap closing.
3. Out-of-plane gap closing.

These are illustrated in figures 19–21 (after [100]).

Note both in-plane configurations create two variable capacitors with the capacitances 180° out of phase. The three approaches can be operated either in charge constrained or voltage constrained cycles. In general the voltage constrained offers more energy than the charge constrained approach. However, by incorporating a capacitor in parallel with the energy harvesting capacitor, the energy from the charge constrained system can approach that of the voltage constrained system as the parallel capacitance approaches infinity. This parallel capacitor effectively constrains the voltage on the energy harvesting capacitor [98].

Table 2 provides the electrostatic force variation for the three configurations where x is the displacement of the inertial mass [99]. For a high damping configuration the electrostatic damping force has to be counter-balanced almost entirely by the mechanical spring force [99].

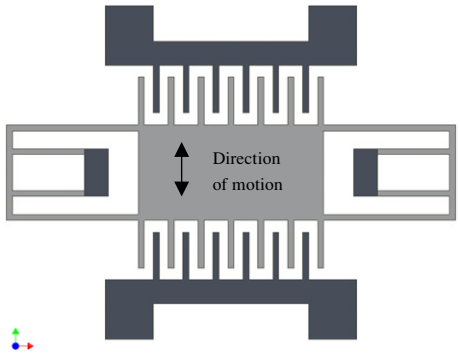

Figure 19. In-plane overlap varying.

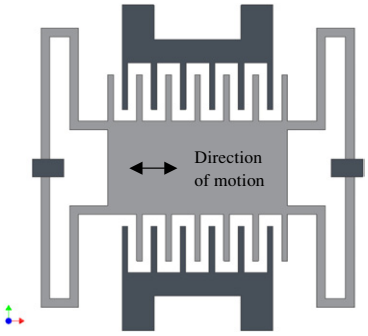

Figure 20. In-plane gap closing.

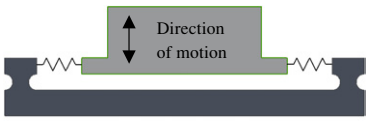

Figure 21. Out-of-plane gap closing.

Table 2. Electrostatic force variation for the three configurations.

Structure	Charge constrained	Voltage constrained
In-plane overlap varying	$F_e \sim 1/x^2$	F_e constant
In-plane gap closing	$F_e \sim x$	$F_e \sim 1/x^2$
Out-of-plane gap closing	F_e constant	$F_e \sim 1/x$

Roundy [100] states that in-plane gap closing offers the highest power output with an optimized design producing 100 μW cm^{-3}; out-of-plane gap closing is the next highest followed by in-plane overlap varying. Maximum power generation occurs for very small dielectric gaps.

5.3. In-plane overlap varying type

Meninger *et al* [101] simulated an in-plane overlap varying electrostatic generator based on a comb-driven structure and generated 8 μW from 2.5 kHz input motion. The operational limit on the electrostatic generator is the potentially high

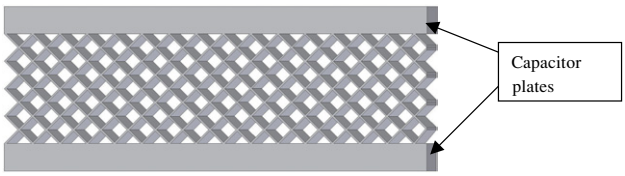

Figure 22. Honeycomb-type variable capacitor.

voltage levels produced. An integrated circuit process was used and limited to the voltage of 8 V in this structure. It was necessary to charge and discharge the generator at specific points in the cycle so a sophisticated energy feedback technique was used whereby the timings were altered depending upon the energy generated.

For their charged floating gate generator Ma [102] predicts a generated 1 μW into an optimum 58 MΩ load for a 5 μm displacement at 4.3 kHz (corresponding to an acceleration of 1825 m s^{-2}). The inertial mass is 2×10^{-7} kg and the device is operated at resonance with a damping coefficient β of 0.002 kg s^{-1}. The single wafer device uses an integrated insulated poly silicon floating gate to provide the bias voltage which is required for operation. The floating gate is charged by electron tunnelling and power is generated by a variable capacitor of which one plate is a moving gold proof mass and the other is the fixed floating gate. An array of 20 devices produced a maximum power of 65 nW at 4.2 kHz at a displacement of 2.2 μm (equivalent acceleration 766 m s^{-2})

5.4. In-plane gap closing type

Despesse [99] reports on an electrostatic transduction structure with high electrical damping designed to operate over a wide low frequency range (<100 Hz). The structure chosen is an in-plane gap closing structure with a charge constrained cycle. In this case the electrostatic force is linearly proportional to the inertial mass displacement in the same way as is the mechanical spring force. This allows the two forces to be balanced for all displacements of the inertial mass. A high electrical damping is therefore achieved by choosing the electrical stiffness close to the mechanical stiffness. An 18 cm^2 $\times$ 1 cm volume device with a 0.104 kg inertial mass was electro discharge machined from tungsten and produced a scavenged power of 1052 μW for a vibration amplitude of 90 μm at 50 Hz (corresponding to an acceleration of 8.8 m s^{-2}). This represents a scavenged efficiency of 60% with the losses being accounted for by charge/discharge losses and transduction losses. A similar geometry silicon microstructure of volume 81 mm^2 $\times$ 0.4 mm with a 2×10^{-3} kg inertial mass excited by a vibration amplitude of 95 μm at 50 Hz is predicted to produce a scavenged power of 70 μW.

5.5. Out-of-plane gap closing type

Tashiro [103] describes a honeycomb structure as shown in figure 22 made up by folding a strip of a polyester film with aluminium evaporated on one surface. Two sheets of the film each 5 μm thick by 30 mm wide and 5 m long were mated together using a double-sided adhesive tape at 5 mm intervals. Then the sheets were folded and joined again using a double-sided tape. This produced a variable capacitor with 20 cells per layer and 50 layers resulting in 100 cells. The capacitor was suspended between acrylic boards using 12 springs and an inertial mass attached to one of the acrylic boards. The spring constant of the resonator was 1100 N m^{-1} with a total mass of 0.78 kg resulting in a resonant frequency of 6 Hz.

After initially charging the capacitor to 45 V the generator was shaken at by a simulation of the movement produced by the left ventricular wall motion of a canine heart and produced a mean power of 36 μW (15 μA at 2.4 V) with peak powers as high as 500 μW. Accelerometer measurements showed this movement to be about 1 m s^{-2} at 6 Hz.

Earlier experiments by the same team [104] reported the generation of 58 μW from the simulated heart movements of a goat after an initial charging voltage of 24 V. They used a similar structure honeycomb generator which had an initial capacitance of 32 nF varying to 200 nF and was resonant at 4.76 Hz. This was driven at a harmonic of the fundamental frequency of the heart, this being 1 to 2 Hz, although frequencies up to 10 Hz were present in the motion. In this study the inertial mass was 1.2 kg and the resonator spring constant was 570 N m^{-1}. The resonator was tuned to the application vibration's frequency by adjusting the mass.

Miyazaki [105] presented an out-of-plane cantilever-based generator with a base capacitance of 1 nF and a variable capacitance of between 30 pF and 350 pF. The device resonated at 45 Hz with a Q factor of 30. The device was tested on a wall with a 1 μm displacement up to 100 Hz. 120 nW was harvested for the wall acceleration of 0.08 m s^{-2}.

5.6. Coulomb force parametric generator

Miao [106] and Mitcheson [107] describe a non-resonant electrostatic generator designed to operate in applications in which the amplitude of the external motion is larger than the maximum internal displacement of the proof mass of the generator. The 10^{-4} kg proof mass is designed to move only during the portion of the motion cycle when the acceleration is at a maximum. The device has four phases of operation: prime, wait, flight and discharge. The three-wafer device (glass, silicon, glass) consists of a moving silicon proof mass attached to silicon frame by a polyimide suspension, a bottom plate containing the counter electrode and discharging studs and a top plate containing the discharge contacts.

Initially, in the priming phase, the proof mass is held against the charging studs by a priming voltage of the order of 100 V which must be provided externally. The force induced by the priming voltage is chosen to be just below the inertial force produced by the maximum acceleration in the application being addressed. When the inertial force is above the holding force the mass separates from the charging plate and moves towards the discharge contacts at constant charge—this is the flight phase. The work done in separation increases the capacitor's voltage until, at maximum displacement, the moving plate touches the discharging circuit.

The stored energy ($0.5CV^2$) increases by the ratio of the initial to final capacitance. Hence the initial capacitance must be maximized by minimizing the gap between the moving plate and the counter electrode. This also has the effect of

decreasing the required priming voltage for a given holding force. The device is 20 mm × 25 mm by 1.5 mm thick and the charge capacitor spacing is about 6 μm giving a capacitance of 150 pF. The discharge capacitance is 5.5 pF. The device produces output voltages up to 220 V corresponding to a net generated power of 120 nJ per cycle for accelerations of the order of 50 m s^{-2}. Theory predicts 2.6 μJ per cycle, equivalent to 80 μW, is achievable for this device size at 30 Hz and 10 m s^{-2} acceleration; the practical limitation is believed to be the tilting motion of the inertial mass as well as parasitic capacitances. Sufficient flexibility is required in the desired direction of movement with sufficient stiffness in undesired movement directions to minimize the tilting problem. The structure, when compared to a comb structure, gives a higher initial capacitance and a higher capacitance ratio between the two end conditions of the capacitor The stored energy increase can also be increased by minimizing the discharge capacitance but this must be kept larger than any parasitic capacitances to ensure that the majority of the energy is discharged in the discharge capacitor. The extraction circuitry must handle hundreds of volts at low leakage and with low parasitic capacitance values.

5.7. Generators using charged electrets

Sterken [108, 109] presents a concept of an in-plane, overlap varying, voltage constrained, variable capacitor polarized with a SiO_2/Si_3Ni_4 electret. Maximum power is achieved by

1. maximizing the capacitance change per unit displacement of the inertial mass;
2. tuning the damping until the inertial mass displacement is at the maximum permitted by the structure;
3. maximizing the polarization voltage 300 V is achieved in the realized device.

The device is bulk micromachined from two silicon wafers (inertial mass and electret) and one glass wafer (fixed electrode) the latter being used to reduce parasitic capacitances.

Arakawa [110] presents an in-plane, overlap varying, voltage constrained, variable capacitor polarized with a fluorocarbon polymer electret offering high dielectric strength. For a 1 mm displacement amplitude at 10 Hz (corresponding to an acceleration of 3.94 m s^{-2}), a 20 mm × 20 mm × 2 mm two-wafer glass device produces 6 μW at 200 V into an optimized external load of 10^8 Ω.

Peano [111] numerically analyses an electret-based in-plane overlap varying surface micromachined structure. They show that nonlinear behaviour of the converter is crucial in the optimization of the generator and has to be taken into account. A power of 50 μW is predicted from a 911 Hz vibration source moving 5 μm which corresponds to an acceleration of 164 m s^{-2}. The same device optimized with a linear model is expected to produce a power of 5.8 μW.

Mizuni and Chetwynd [85] present an electret-based out-of-plane, gap closing, voltage constrained variable capacitor. For a 400 μm × 50 μm × 10 μm cantilever with a 100 μm air gap and an excitation of 100 nm at 28 kHz (corresponding to an acceleration of 3095 m s^{-2}) theory predicts an EMF of 97 mV.

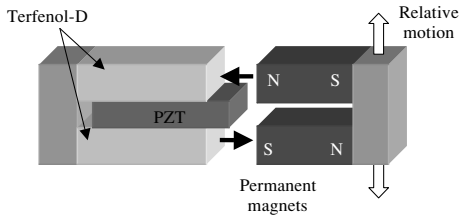

Figure 23. Linear vibration powered magnetostrictive-piezoelectric composite generator.

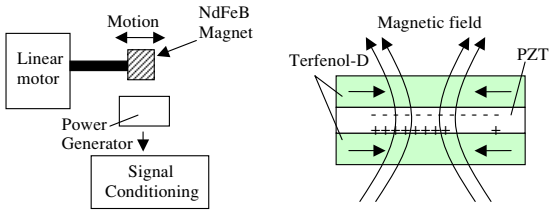

Figure 24. Laminated structure and experimental structure.

6. Other methods

Magnetostrictive materials also possess suitable characteristics. These materials deform when placed in a magnetic field and conversely if strained can induce changes in a magnetic field. Magnetostrictive materials can be used independently but have more typically been employed in piezoelectric-magnetostrictive composites. Such composites were originally intended for use in magnetic field sensors but have more recently been evaluated for use in energy-harvesting applications.

Huang *et al* have detailed two designs of an energy harvesting device based upon a Terfenol-D/PZT/Terfenol-D composite [112]. The first variation is shown in figure 23 where a horseshoe arrangement of permanent magnets moves linearly relative to a fixed composite.

The second arrangement described by Huang *et al* couples linear vibrations into rotary motion of a circular composite disc placed within a magnetic field. The frequency of the rotary resonance depends upon the spring constant of the springs that control the motion of the disc and the size of the eccentric proof mass used to achieve rotary motion. This device achieved 1.2 mW of power at 30 Hz at 5 m s^{-2} and claims were made that more than 10 mW could be harvested from a volume of 1 cm^3 at 5 m s^{-2}. The volumes quoted in the paper, however, were of the composite sandwich and did not include the required mass, magnets, springs and housing which should not be ignored.

Bayrashev *et al* also fabricated a diameter of 0.5 mm thick PZT disc sandwiched between 1.5 mm thick Terfenol discs [113]. When the laminate is exposed to a low frequency (<100 Hz) varying magnetic field, the PZT layer was similarly strained and a charge generated. The orientation of the laminated layers and the experimental set-up is shown in figure 24. A neodymium iron boron (NdFeB) magnet was attached to a linear motor and moved laterally at various frequencies. Power output was found to be between 10 and 80 μW depending upon the distance between the magnet and the composite. The optimum thickness of PZT will depend upon the Terfenol-D thickness and its ability to maximize the

strain within the PZT. Two layers of Terfenol-D were found to produce 35% more voltage than a single layer due to the increased level of strain in the PZT layer. Generator efficiency was calculated to be 3.1% due to the accumulated losses in the various transduction processes.

7. Comparison of transduction mechanisms

The efficiency of a generator should be simply defined by the standard definition, $\eta = U_{out}/U_{in}$ where U_{out} is the energy delivered to an electrical load and U_{in} is the input energy from the excitation vibrations per cycle. A recent paper by Roundy [114] has proposed a method based upon a standard two-port model of a transducer which enables the different transduction mechanisms to be compared [115]. The analysis uses a coupling coefficient, κ, which is a measure of the efficiency of the conversion from the external vibration energy to the energy stored within the generator and transmission coefficient, λ, which is mathematically identical to the equation for efficiency given above. The transmission coefficient is related to the coupling coefficient and λ_{max} can be found from

$$\lambda_{max} = \frac{k^2}{4 - 2k^2}. \tag{28}$$

In practice the transmission coefficient depends upon the load resistance which should be chosen to achieve λ_{max}. The maximum power can be found from equation (29) where ω is the circular frequency of driving vibrations:

$$P_{max} = \lambda_{max}\omega U_{in}. \tag{29}$$

These coefficients have been derived by Roundy for each of the transduction mechanisms and can be employed to compare them as follows. In the case of the electromagnetic generator, the coupling factor is given by

$$\kappa^2 = \frac{(Bl)^2}{k_{sp}L}, \tag{30}$$

where B is the magnetic field, l is the length of the wire in the coil, k_{sp} the spring constant and L the coil inductance. For piezoelectric generators equation (31) applies where d is the piezoelectric strain coefficient (see section 2.1), E is Young's modulus and ε is the dielectric constant:

$$\kappa^2 = \frac{d^2 E}{\varepsilon}. \tag{31}$$

The maximum energy density for both electromagnetic and piezoelectric generators is given by

$$p_{max} = \frac{\kappa^2 \rho (QA)^2}{4\omega}, \tag{32}$$

where ρ is the density of the proof mass material, Q is the quality factor of the generator, and A the magnitude of acceleration of the excitation vibrations. The solutions for electrostatic generators are nonlinear and depend upon the geometry and operating conditions of the device. Taking the example of a out-of-plane parallel plate capacitor operating in a constant charge mode as described in section 4.2:

$$\kappa^2 = \frac{V_{in}^2 C_{max}^2}{V_{in}^2 C_{max}^2 + m\omega^2 z^2 C(z)}. \tag{33}$$

Equation (33) gives the coupling coefficient where V_{in} is the input voltage, z the displacement of the top electrode and C_{max} is the maximum capacitance. It is clear the capacitance varies with displacement and therefore the coupling coefficient varies throughout the cycle. The average power output density is given by equation (34) where f is the generator frequency in Hz.

$$p_{ave} = f\frac{\rho (QA)^2}{4\omega^2}\int_{t1}^{t2} \kappa(t)\,\mathrm{d}t. \tag{34}$$

The coupling coefficient of piezoelectric generators depends primarily on the piezoelectric material used, although the elastic properties of the other materials used in the generator structure may also influence the values. Roundy has calculated the coefficients for common piezoelectric materials and these are shown in table 3.

Table 3. Coupling and transmission coefficients for common piezoelectric materials (after [114]).

Material	κ_{33}	κ_{31}	λ_{33}	λ_{31}
PZT-5A	0.72	0.32	0.175	0.027
PZT-5H	0.75	0.44	0.196	0.054
PVDF	0.16	0.11	0.006	0.003
PZN-PT	0.91	0.5	0.353	0.071

The coupling coefficient of electromagnetic generators is dependant upon the design of the device. Roundy has plotted transmission and coupling coefficient contours against frequency and area enclosed by the conductor loop and has assumed a proof mass density of 7.5 g cm^{-3} and a magnetic flux density (B) of 0.1 T. Given these values, Roundy has concluded that possible coupling coefficients for electromagnetic generators are comparable to those for piezoelectric devices (shown in table 3). Since equation (33) applies to both generator types, the maximum power density will be comparable. In the case of electrostatic generators the coupling coefficient varies with position and device design. To illustrate a typical case, Roundy has plotted average coupling factor versus frequency and gap for a 1 cm^2 parallel plate device with a proof mass density of 7.5 g cm^{-3} and a Q of 30. Again coefficients appear similar in value to those shown in table 3, but actually achieving higher coefficients requires impractically large amplitudes of displacement compared to the minimum capacitor separation gap.

8. Conclusions and future possibilities

There is little doubt that the field of vibration energy harvesting continues to expand apace. With the predicted proliferation of wireless sensor networks, an alternative (or at least complementary) approach to battery power is required. If there are sufficient ambient vibrations available, then it is possible to generate an electrical supply by using a micro-generator to harvest the mechanical excitation. There are three main approaches that can be used to implement a vibration-powered generator. Each of the technologies described in this review has their own advantages and disadvantages and these are now summarized.

8.1. Piezoelectric generators

These offer the simplest approach, whereby structural vibrations are directly converted into a voltage output by using

Table 4. Summary of piezoelectric generators.

Reference	P (μW)	F (Hz)	A (m s^{-2})	M (g)	Volume (mm^3)	Details
Kymissis [44] MIT (US)	1300	0.9	–	–	16 000[a]	PVDF stack located on shoe insole driven by a walking human
Umeda [38]	19[a] (per impact)	N/A	N/A	1.73	214	Bronze/PZT disc driven by impacts
Shenk [45] MIT (US)	8400	0.9	N/A	N/A	25 000[a]	PZT dimorph located in heal of shoe driven by a walking human
Ramsay [50]	2.3	1				1.1 mm × 1 cm × 1 cm
White [55] Southampton University (UK)	2.1	80.1	2.3[a]	0.8	125	Steel/screen printed PZT
Roundy [20] Berkeley University (US)	210	120	2.5	8.5[a]	1000	Brass/PZT/tungsten cantilever generator
Roundy [20] Berkeley University (US)	375	120	2.5	9.2[a]	1000	Brass/PZT/tungsten cantilever generator
Sodano [60] Virginia Poly (US)	11.9	30	Not stated	9.52	Total device 1947, active volume 240	Mide Technology QP40 N transducer clamped at one end
Duggirala [68] Cornell University (US)	0.001	35	N/A	N/A	60[a]	^{63}Ni radioisotope Silicon/PZT cantilever
Bayrashev [113] Minnesota University (US)	80	5	Not stated	15.6[a] (including magnet)	2185 (including magnet)	Terfenol-D/PZT/ Terfenol-D composite
Marzencki [69] Tima, France	0.1[b] AIN 0.6[b] PZT	900	9.81	1.1×10^{-3}	2 (whole chip) 0.9 (mass and cantilever)	Thin film AIN or PZT on micromachined silicon cantilever structure
Jeon [70] Varian Korea, Korea IST, Polychromix and MIT (US)	1	13.9	106	Not given	0.027[a]	Micromachined silicon device with IDT electrodes

[a] Estimated or extrapolated from data in reference.
[b] Simulated results.

an electroded piezoelectric material. There is no requirement for having complex geometries and numerous additional components. Piezoelectric generators are the simplest type of generator to fabricate and can be used in force and impact-coupled harvesting applications. There is a wide range of piezoelectric materials available for different application environments. One major advantage is that this transduction principle is particularly well suited to microengineering, since several processes exist for depositing piezoelectric films (thin and thick). The piezoelectric method is capable of producing relatively high output voltages but only at low electrical currents.

The piezoelectric materials are required to be strained directly and therefore their mechanical properties will limit overall performance and lifetime. Also the transduction efficiency is ultimately limited by piezoelectric properties of materials employed. The output impedance of piezoelectric generators is typically very high (>100 kΩ). Table 4 summarizes the main characteristics of piezoelectric generators.

8.2. Electromagnetic generators

These offer a well-established technique of electrical power generation and the effect has been used for many years in a variety of electrical generators. There is a wide variety of spring/mass configurations that can be used with various types of material that are well suited and proven in cyclically stressed applications. Comparatively high output current levels are achievable at the expense of low voltages (typically <1 V). High-performance bulk magnets and multi-turn, macro-scale coils are readily available.

Wafer-scale systems, however, are quite difficult to achieve owing to the relatively poor properties of planar magnets, the limitations on the number of turns achievable with planar coils and the restricted amplitude of vibration (hence magnet/coil velocity). Inevitably, there are also problems associated with the assembly and alignment of sub-millimetre scale electromagnetic systems. Table 5 summarizes the main characteristics of electromagnetic generators.

8.3. Electrostatic generators

The electrostatic concept is easily realizable as a MEMS and much processing know-how exists on the realization of in-plane and out-of-plane capacitors. Energy density of the generator can be increased by decreasing the capacitor spacing, facilitating miniaturization. The energy density, however, is also decreased by reducing the capacitor surface area. High transduction damping, at low frequencies, is achievable by incorporating small capacitor gaps and high voltages.

Unfortunately, electrostatic generators require an initial polarizing voltage or charge. This is not an issue in applications that use the generator to charge a battery, as this can be used to provide the necessary initial excitation level. Electrostatic generators can utilize electrets to provide the initial charge and these are capable of storing charge for many years. The output impedance of the devices is often very high and this makes them less suitable as a power supply. The output voltage produced by the devices is relatively high (>100 V) and often results in a limited current-supplying

Table 5. Summary of electromagnetic generators.

Reference	P (μW)	F (Hz)	A (m s^{-2})	Mass (g)	Volume	Material
Shearwood [81, 84]	0.3	4400	382	0.0023	5.4 mm^3	GaAs
Sheffield University (UK)						Polyimide
Amarithajah [92]	400[a]	94	–	0.5	–	Discrete components
MIT (US)						
El-hami [24]	530	322	–	–	0.24 cm^3	Steel
Southampton University (UK)						
Mizuno 2003 [85]	0.4 nW	700	12.4	–	2.1 cm^3[a]	Silicon
Warwick University (UK)						
Glynne-Jones [91]	180	322	2.7	–	0.84 cm^3	Steel
Southampton University (UK)						
Perpetuum [96]	4000	100	0.4	50	30 cm^3	Steel
UK company						
Kulah [86]	2.5[a]	11400	–	–	4 mm^3	Silicon/parylene
Michigan University (US)	4 nW	25			2 cm^3	Silicon/styrene
Huang [87]	0.16	100	'Finger tap'	–	–	Copper
Tsing Hua University (Taiwan)						
Pérez-Rodríguez [88] Barcelona University (Spain)	1.44	400	–	–	250 mm^3	Polyimide
Beeby [90]	0.5	9500	1.92	0.028	–	Silicon
Southampton University (UK)						
Li [93]	10	64	16.16[a]	–	1 cm^3	Copper/brass
Hong Kong University (China)						
Ching [94]	830	110	95.5[a]	–	1 cm^3	Copper/brass
Hong Kong University (China)						
Scherrer [89]	7000	35	–	–	9 cm^3	LTCC/beryllium/copper
Boise State University (US)						

[a] Simulated results.

Table 6. Summary of electrostatic generators

Reference	P (μW)	F (Hz)	A (m s^{-2})	M (g)	Volume (mm^3)	Details
Tashiro [104]	58	4.76	0.5	1200	–	Aluminium/polyester
Terumo Corp (Jp)						
Meninger [101]	8[2]	2520	–	–	75	Silicon
MIT (US)						
Tashiro [103]	36	6	1	780	–	Aluminium/polyester
Terumo Corp (Jp)						
Mitcheson [107]	3.7	30	50	0.1	750	Silicon/pyrex
Imperial College (UK)						
Sterken [108, 109]	100[a]	1200	1137	–	–	Silicon/pyrex
IMEC (B)						
Roundy [100]	110[a]	120	2.25	–	1000	Silicon
Berkeley University (US)						
Chetwynd [85]	97 mV	28000	1395	–	–	Aluminium/gold/glass
Warwick University (UK)						
Miyazaki [105]	0.12	45	0.08	–	–	Metal
Hitachi [Jp]						
Ma [102]	0.065	4200	766	2×10^{-4}	–	Gold/silicon
Hong Kong University (China)						
Arakawa [110]	6	10	3.9	–	800	Polymer/glass
Tokyo University (Jp)						
Despesse [99]	1052	50	8.8	104	1800	Tungsten
LETI (F)						
Despesse [99]	70[(1)]	50	9.2	2	32.4	Silicon
LETI (F)						
Peano [111]	50[a]	911	164	–	–	Silicon
Turin Polytecnicoo (I)						

[a] Simulated results.

capability; this can lead to the requirement for custom circuit implementation processes for the realization of challenging circuit designs. Parasitic capacitances within the structure can sometimes lead to reduced generator efficiency and there is risk of capacitor electrodes shorting or of 'stiction' in wafer-scale implementations. Table 6 summarizes the main characteristics of electrostatic generators.

The three main techniques of harvesting energy from ambient vibrations have been shown to be capable of generating output power levels in the range of μW to mW. A

few years ago, such energy levels would have been considered as 'unusable'. Modern-day VLSI circuit designs, however, are being built with low-power operation in mind and many commercial circuits can now be used with energy harvesting solutions. Take, as an example, the electronic calculator whose early form required several 'AA' sized cells, but are now capable of running wholly off solar power.

Vibration-powered wireless sensor systems can be used in numerous scenarios and several research groups across the world are addressing possible uses in ambient intelligence, medical implants and smart clothing. Wireless, battery-less industrial condition monitoring systems are already close to commercialization.

References

[1] Bult K *et al* 1996 A distributed, wireless MEMS technology for condition based maintenance *Proc. 1996 Integrated Monitoring, Diagnostics and Failure Prevention Conference, Society of Machine Failure Protection Technology (MPFT) (Mobile, AL, USA)* pp 373–80

[2] Raghunathan V, Schurgers C, Park S and Skrivastava M B 2002 Energy-aware wireless microsensor networks *IEEE Signal Process. Mag.* **19** 40–50

[3] Enz C C, El-Hoiydi A, Decotignie J-D and Peiris V 2004 WiseNET: An ultralow-power wireless sensor network solution *IEEE Comput.* **37** 62–70

[4] Warneke B, Last M, Leibowitz B and Pister K S J 2001 Smart dust: communicating with a cubic-millimeter computer *IEEE Comput.* **34** 44–51

[5] Callahan E H Jr 2004 *Wireless Sensor Networks* (Boca Raton, FL: CRC Press)

[6] IEEE 802.15.4 Standard 2003 (New York: IEEE)

[7] Frank R 2004 Move over, Bluetooth; ZigBee is here *Design News* **4** (http://www.designnews.com/article/CA387448.html)

[8] Rabaye J, Ammer M J, da Silva J L, Patel D and Roundy S 2000 Picoradio supports ad hoc ultra-low power wireless networking *IEEE Comput.* **33** 42–8

[9] Brignell J E and White N M 1996 *Intelligent Sensor Systems* (Bristol: Institute of Physics Publishing)

[10] Banazwski B and Shah R K 2003 The role of fuel cells for consumer electronic products and toys *Proc. 1st Int. Conf. on Fuel Cell Science, Engineering and Technology (Rochester, NY, USA)* pp 149–55

[11] Epstein A H 2004 Millimeter-scale, micro-electro-mechanical systems gas turbine engines *J. Eng. Gas Turbines Power* **126** 205–26

[12] Tanaka S, Changa K-S, Mina K-B, Satoh D, Yoshida K and Esashi M 2004 MEMS-based components of a miniature fuel cell/fuel reformer system *Chem. Eng. J.* **101** 143–9

[13] Koeneman P B, Busche-Vishniac I J and Wood K L 1997 Feasibility of micro power supplies for MEMS *IEEE J. Microelectomech. Syst.* **6** 355–62

[14] Görge G, Kirstein M and Erbel R 2001 Microgenerators for energy autarkic pacemakers and defibrillators: fact or fiction *Herz* **26** 64–8

[15] Amirtharajah R and Chandrakasan A P 1998 Self-powered signal processing using vibration-based power generation *IEEE J. Solid State Circuits* **33** 687–95

[16] Jacobson S A and Epstein A H 2003 An informal survey of power MEMS *Proc. Int. Symp. on Micro-Mechanical Engineering ISMME (Japan)* p K18

[17] Kiely J J, Morgan D V and Rowe D M 1991 Low cost miniature thermoelectric generator *Electron. Lett.* **27** 2332–4

[18] Schaevitz S B, Franz A J, Jensen K F and Schmidt M A 2001 A combustion-based MEMS thermoelectric power generator *Proc. 11th Int. Conf. on Solid-State Sensors and Actuators, Transducers 01 (Munich, Germany)* p 1A3-02

[19] Zhang C, Najafi K, Bernal L P and Washabaugh P D 2001 An integrated combustor-thermoelectric micro power generator *Proc. 11th Int. Conf. on Solid-State Sensors and Actuators, Transducers 01 (Munich, Germany)* p 1A3–03

[20] Roundy S, Wright P K and Rabaye J 2003 A study of low level vibrations as a power source for wireless sensor nodes *Comput. Commun.* **26** 1131–44

[21] Starner T and Paradiso J A 2004 Human generated power for mobile electronics *Low Power Electronics Design,* ed C Piguet (Boca Raton, FL: CRC Press)

[22] von Büren T, Lukowicz P and Tröster G 2003 Kinetic energy powered computing—an experimental feasibility study *Proc. 7th IEEE Int. Symposium on Wearable Computers ISWC '03 (White Plains, NY)* pp 22–4

[23] Williams C B and Yates R B 1996 Analysis of a micro-electric generator for microsystems *Sensors Actuators* A **52** 8–11

[24] El-Hami M, Glynne-Jones P, James E, Beeby S P, White N M, Brown A D, Ross J N and Hill M 2001 Design and fabrication of a new vibration-based electromechanical power generator *Sensors Actuators* A **92** 335–42

[25] Stephen N G 2006 On energy harvesting from ambient vibration *J. Sound Vib.* **293** 409–25

[26] Roundy S J 2003 Energy scavenging for wireless sensor nodes with a focus on vibration to electricity conversion *PhD Thesis* University of California

[27] Mitcheson P D, Green T C, Yeatman E M and Holmes A S 2004 Architectures for vibration-driven micropower generators *IEEE J. Microelectomech. Syst.* **13** 429–40

[28] Baudry H 1987 Screen-printing piezoelectric devices *Proc. 6th European Microelectronics Conference (London, UK)* pp 456–63

[29] White N M and Turner J D 1997 Thick-film sensors: past, present and future *Meas. Sci. Technol.* **8** 1–20

[30] Lovinger A J 1983 Ferroelectric polymers *Science* **220** 1115–21

[31] Nye J F 1957 *Physical Properties of Crystals* (Oxford: Oxford University Press)

[32] Richards C D, Anderson M J, Bahr D F and Richards R F 2004 Efficiency of energy conversion for devices containing a piezoelectric component *J. Micromech. Microeng.* **14** 717–21

[33] Goldfarb M and Jones L D 1999 On the efficiency of electric power generation with piezoelectric ceramic *Trans. ASME J. Dyn. Syst. Meas. Control* **121** 566–71

[34] IEEE Standard on Piezoelectricity 1987 ANSI/ IEEE Standard 176-1987

[35] *Piezoelectric Ceramics Data Book for Designers* Morgans Electroceramics

[36] Gonzalez J L, Rubio A and Moll F 2001 A prospect of the piezoelectric effect to supply power to wearable electronic devices *Proc. 4th Int. Conf. on Materials Engineering for Resources (Akita, Japan)* pp 202–07

[37] Umeda M, Nakamura K and Ueha S 1996 Analysis of the transformation of mechanical impact energy to electric energy using piezoelectric vibrator *Japan. J. Appl. Phys.* **35** 3267–73

[38] Umeda M, Nakamura K and Ueha S 1997 Energy storage characteristics of a piezo-generator using impact induced vibrations *Japan. J. Appl. Phys.* **36** 3146–51

[39] Cavallier B, Nouira H, Foltete E, Hirsinger L and Ballandras S 2005 Energy storage capacity of vibrating structure: application to a shock system *Proc. Symp. on Design, Test, Integration and Packaging of MEMS/ MOEMS DTIP05 (Montreux, Switzerland)* pp 391–3

[40] Xu C-N, Akiyama M, Nonaka K and Watanabe T 1998 Electrical power generation characteristics of PZT piezoelectric ceramics *IEEE Trans. UFFC* **45** 1068–70

[41] Funasaka T, Furuhata M, Hashimoto Y and Nakamura K 1999 Piezoelectric generator using a $LiNbO_3$ plate with an

inverted domain *IEEE Ultrasonics Symp. (Honolulu, HI)* pp 959–62
[42] Starner T 1996 Human-powered wearable computing *IBM Syst. J.* **35** 618–29
[43] Antaki J F, Bertocci G E, Green E C, Nadeem A, Rintoul T, Kormos R L and Griffith B P 1995 A gait powered autologous battery charging system for artificial organs *Am. Soc. for Artif. Internal Organs J.* **41** M588–95
[44] Kymissis J, Kendall C, Paradiso J and Gershenfeld N 1998 Parasitic power harvesting in shoes *Proc. 2nd IEEE Int. Conf. Wearable Computing (California)* pp 132–9
[45] Shenck N S and Paradiso J A 2001 Energy scavenging with shoe-mounted piezoelectrics *IEEE Micro.* **21** 30–42
[46] Hellbaum R F, Byrant R G and Fox R L 1997 Thin layer composite unimorph ferroelectric driver and sensor *US Patent* 5632841
[47] Yoon H-S, Washington G and Danak A 2005 Modelling, optimisation, and design of efficient initially curved piezoceramic unimorphs for energy harvesting applications *J. Intell. Mater. Syst. Struct.* **16** 877–88
[48] Mateu L and Moll F 2005 Optimum piezoelectric bending beam structures for energy harvesting using shoe inserts *J. Intell. Mater. Syst. Struct.* **16** 835–45
[49] Drake J 2001 The greatest shoe on Earth *Wired* **9** 90–100
[50] Ramsay M J and Clark W W 2001 Piezoelectric energy harvesting for bio MEMS applications *Proc. SPIE* **4332** 429–38
[51] Sohn J W, Choi S B and Lee D Y 2005 An investigation on piezoelectric energy harvesting for MEMS power sources *Proc. IMechE 219 Part C J. Mech. Eng. Sci.* pp 429–36
[52] Platt S R, Farritor S, Garvin K and Haider H 2005 The use of piezoelectric ceramics for electric power generation within orthopedic implants *IEEE/ASME Trans. Mechatron.* **10** 455–61
[53] Renaud M, Sterken T, Fiorini P, Puers R, Baert K and van Hoof C 2005 Scavenging energy from human body: design of a piezoelectric transducer *Tech. Digest 13th Int. Conf. on Solid-State Sensors and Actuators Transducers '05 (Seoul, Korea)* vol 1, pp 784–7
[54] White N M, Glynne-Jones P and Beeby S P 2001 A novel thick-film piezoelectric micro-generator *Smart Mater. Struct.* **10** 850–2
[55] Glynne-Jones P, Beeby S P and White N M 2001 Towards a piezoelectric vibration powered microgenerator *IEE Proc.—Sci. Meas. Technol.* **148** 68–72
[56] Glynne-Jones P, Beeby S P and White N M 2001 The modelling of a piezoelectric vibration powered generator for microsystems *Proc. 11th Int. Conf. on Solid-State Sensors and Actuators, Transducers 01 (Munich, Germany)* pp 46–9
[57] Beeby S P, Blackburn A and White N M 1999 Processing of PZT piezoelectric thick films on silicon for microelectromechanical systems *J. Micromech. Microeng.* **9** 218–29
[58] Torah R, Beeby S and White N 2005 An improved thick-film piezoelectric material by powder blending and enhanced processing parameters *IEEE Trans. UFFC* **52** 10–16
[59] Roundy S and Wright P K 2004 A piezoelectric vibration based generator for wireless electronics *Smart Mater. Struct.* **13** 1131–42
[60] Sodano H A, Park G and Inman D J 2004 Estimation of electric charge output for piezoelectric energy harvesting *Strain* **40** 49–58
[61] http://www.mide.com/prod_energy_harvester.html
[62] Sodano H A, Magliula E A, Park G and Inman D J 2002 Electric power generation using piezoelectric materials *Proc. 13th Int. Conf. on Adaptive Structures and Technologies (Potsdam, Germany)* pp 153–61
[63] Sodano H A, Inman D J and Park G 2004 A review of power harvesting from vibration using piezoelectric materials *Shock Vibration Dig.* **36** 197–206
[64] Lu F, Lee H P and Lim S P 2004 Modeling and analysis of micropiezoelectric power generators for micro-electromechanical-systems applications *Smart Mater. Struct.* **13** 57–63
[65] Ng T H and Liao W H 2005 Sensitivity analysis and energy harvesting for a self-powered piezoelectric sensor *J. Intell. Mater. Syst. Struct.* **16** 785–97
[66] Li H, Lal A, Blanchard J and Henderson D 2002 Self-reciprocating radioisotope-powered cantilever *J. Appl. Phys.* **92** 1122–7
[67] Lal A and Blanchard J 2004 The daintiest dynamics *IEEE Spectr.* **41** 36–41
[68] Duggirala R, Li H, Pappu A M, Fu Z, Aspel A and Lal A 2004 Radioisotope micropower generator for CMOS self-powered sensor microsystems *Proc. 4th Int. Workshop on Micro and Nantechnology for Power Generation and Energy Conversion Applications PowerMEMS 2004 (Kyoto, Japan)* pp 133–6
[69] Marzencki M, Basrour S, Charlot B, Grasso A, Colin M and Valbin L 2005 Design and fabrication of piezoelectric micro power generators for autonomous microsystems *Proc. Symp. on Design, Test, Integration and Packaging of MEMS/MOEMS DTIP05 (Montreux, Switzerland)* pp 299–302
[70] Jeon Y B, Sood R, Jeong J-h and Kim S G 2005 MEMS power generator with transverse mode thin film PZT *Sensors Actuators* A **122** 16–22
[71] Sodano H A, Park G, Leo D J and Inman D J 2003 Use of piezoelectric energy harvesting devices for charging batteries *Proc. SPIE 10th Annual Int. Symp. on Smart Structures and Materials (San Diego, CA, USA)* pp 101–8
[72] Sodano H A, Park G and Inman D J 2003 An investigation into the performance of macro-fiber composites for sensing and structural vibration application *Mech. Syst. Signal Process.* **18** 683–97
[73] Wilkie W K, Bryant R G, High J W, Fox R L, Hellbaum R F, Jalink A, Little B D and Mirick P H 2000 Low cost piezocomposite actuator for structural control applications *Proc. 7th SPIE Int. Symp. on Smart Structures and Materials (Newport Beach, CA)* pp 323–34
[74] Sodano H A, Lloyd J and Inman D J 2004 An experimental comparison between several active composite actuators for power generation *Proc. SPIE* **5390** 370–78
[75] Sodano H A, Inman D J and Park G 2005 Comparison of piezoelectric energy harvesting devices for recharging batteries *J. Intell. Mater. Syst. Struct.* **16** 799–807
[76] Elvin N G, Elvin A A and Spector M 2001 A self-powered mechanical strain energy sensor *Smart Matter. Struct.* **10** 293–99
[77] Dogheche K, Cavallier B, Delobelle P, Hirsinger L, Cattan E, Remiens D, Marzencki M, Charlot B, Basrour S and Ballandras S 2005 A bi-stable micro-machined piezoelectric transducer for mechanical to electrical energy transformation *Proc. Symp. on Design, Test, Integration and Packaging of MEMS/MOEMS DTIP05 (Montreux, Switzerland)* pp 303–4
[78] Kim S, Clark W W and Wang Q-M 2005 Piezoelectric energy harvesting with a clamped circular plate: analysis *J. Intell. Mater. Syst. Struct.* **16** 847–54
[79] Kim S, Clark W W and Wang Q-M 2005 Piezoelectric energy harvesting with a clamped circular plate: experimental study *J. Intell. Mater. Syst. Struct.* **16** 855–63
[80] Allen J J and Smits A J 2001 Energy harvesting eel *J. Fluids Struct.* **15** 629–40
[81] Williams C B, Shearwood C, Harradine M A, Mellor P H, Birch T S and Yates R B 2001 Development of an electromagnetic micro-generator *IEE Proc. Circuits Devices Syst.* **148** 337–42
[82] Williams C W and Yates R B 1996 Analysis of a micro-electric generator for microsystems *Sensors Actuators* A **52** 8–11

[83] Williams C W, Woods R C and Yates R B 1996 Feasibility of a vibration powered micro-electric generator *IEE Coll. on Compact Power Sources (London)* 7/1–7/3
[84] Shearwood C and Yates R B 1997 Development of an electromagnetic micro-generator *Electron. Lett.* **33** 1883–4
[85] Mizuno M and Chetwynd D 2003 Investigation of a resonance microgenerator *J. Micromech. Microeng.* **13** 209–16
[86] Kulah H and Najafi K 2004 An electromagnetic micro power generator for low-frequency environmental vibrations *Micro Electro Mechanical Systems—17th IEEE Conf. on MEMS (Maastricht)* pp 237–40
[87] Huang W S, Tzeng K E, Cheng M C and Huang R S 2003 Design and fabrication of a vibrational micro-generator for wearable MEMS *Proc. Eurosensors XVII (Guimaraes, Portugal)* pp 695–7
[88] Pérez-Rodríguez A, Serre C, Fondevilla N, Cereceda C, Morante J R, Esteve J and Montserrat J 2005 Design of electromagnetic inertial generators for energy scavenging applications *Proc. Eurosensors XIX (Barcelona, Spain)* paper MC5
[89] Scherrer S, Plumlee D G and Moll A J 2005 Energy scavenging device in LTCC materials *IEEE Workshop on Microelectronics and Electron Devices, WMED '05* pp 77–8
[90] Beeby S P, Tudor M J, Koukharenko E, White N M, O'Donnell T, Saha C, Kulkarni S and Roy S 2005 Micromachined silicon generator for harvesting power from vibration *Proc. Transducers 2005 (Seoul, Korea)* pp 780–3
[91] Glynne-Jones P, Tudor M J, Beeby S P and White N M 2004 An electromagnetic, vibration-powered generator for intelligent sensor systems *Sensors Actuators* A **110** 344–9
[92] Amirtharajah R and Chandrakasan A P 1998 Self-powered signal processing using vibration-based power generation *IEEE J. Solid-State Circuits* **33** 687–95
[93] Li W J, Wen Z, Wong P K, Chan G M H and Leong P H W 2000 A micromachined vibration-induced power generator for low power sensors of robotic systems *World Automation Congress: 8th Int. Symp. on Robotics with Applications (Hawaii)*
[94] Ching N N H, Wong H Y, Li W J, Leong P H W and Wen Z 2002 A laser-micromachined vibrational to electrical power transducer for wireless sensing systems *Sensors Actuators* A **97–98** 685–90
[95] www.kinetron.nl
[96] www.perpetuum.co.uk
[97] Roundy S, Wright P and Pister K 2002 Micro-electrostatic vibration-to-electricity converters *Proc. IMECE 2002* pp 1–10
[98] Meninger S 1999 A low power controller for a MEMS based energy converter *MSc* Massachusetts Institute of Technology
[99] Despesse G, Jager T, Chaillout J, Leger J, Vassilev A, Basrour S and Chalot B 2005 Fabrication and characterisation of high damping electrostatic micro devices for vibration energy scavenging *Proc. Design, Test, Integration and Packaging of MEMS and MOEMS* pp 386–90
[100] Roundy S 2003 Energy scavenging for wireless sensor nodes with a focus on vibration to electricity conversion *PhD Thesis* University of California, Berkeley
[101] Meninger S, Mur-Miranda J, Lang J, Chandrakasan A, Slocum A, Schmidt M and Amirtharajah R 2001 Vibration to electric energy conversion *IEEE Trans Very Large Scale Integration (VLSI) Syst.* **9** 64–76
[102] Ma W, Wong M and Ruber L 2005 Dynamic simulation of an implemented electrostatic power micro-generator *Proc. Design, Test, Integration and Packaging of MEMS and MOEMS* pp 380–5
[103] Tashiro R, Kabei N, Katayama K, Tsuboi F and Tsuchiya K 2002 Development of a electrostatic generator for a cardiac pacemaker that harnesses the ventricular wall motion *J. Artif. Organs* 239–45
[104] Tashiro R, Kabai N, Katayama K, Ishizuka Y, Tsuboi F and Tsuchiya K 2000 Development of an electrostatic generator that harnesses the motion of a living body *JSME Int. J.* C **43** 916–22
[105] Miyazaki M, Tanaka H, Ono G, Nagano T, Ohkubo N, Kawahara T and Yano K 2003 Electric-energy generation using variable-capacitive resonator for power-free LSI: efficiency analysis and fundamental experiment *ISLPED '03* pp 193–8
[106] Miao P, Micheson P, Holmes A, Yeatmam E, Green T and Stark B 2005 MEMs inertial power generators for biomedical applications *Proc. Design, Test, Integration and Packaging of MEMS and MOEMS* pp 295–98
[107] Mitcheson P, Stark B, Miao P, Yeatman E, Holmes A and Green T 2003 Analysis and optimisation of MEMS on-chip power supply for self powering of slow moving sensors *Proc. Eurosensors XVII (Guimaraes, Portugal)* pp 30–1
[108] Sterken T, Baert K, Puers R and Borghs S Power extraction from ambient vibration *Proc. 3rd Workshop on Semiconductor Sensors and Actuators* pp 680–3
[109] Sterken T, Fiorini P, Baert K, Borghs G and Puers R 2004 Novel design and fabrication of a MEMS electrostatic vibration scavenger *Power MEMS Conference (Kyoto Japan)* pp 18–21
[110] Arakawa Y, Suzuki Y and Kasagi N 2004 Micro seismic power generator using electret polymer film *Power MEMS Conference (Kyoto, Japan)* pp 187–90
[111] Peano F and Tambosso T 2005 Design and optimisation of a MEMS electret-based capacitive energy scavenger *J. Microelectromech. Syst.* **14** 435–529
[112] Huang J, O'Handley R C and Bono D 2003 New, high-sensitivity, hybrid magnetostrictive/electroactive magnetic field sensors *Proc. SPIE* **5050** 229–37
[113] Bayrashev A, Robbins W P and Ziaie B 2004 Low frequency wireless powering of microsystrems using piezoelectric-magnetostrictive laminate composites *Sensors Actuators* A **114** 244–9
[114] Roundy S 2005 On the effectiveness of vibration-based energy harvesting *J. Intell. Mater. Syst. Struct.* **16** 809–23
[115] Bright C 2001 Energy coupling efficiency *Sensors* **18** (6) (http://archives.sensorsmag.com/articles/0601/76/index.htm)